Cluster Model Investigation of Nuclear Spectra and Electric Quadrupole Transitions

Vanessa A. McBride

December 2003

Thesis submitted in fulfilment of
the requirements for the degree of Master of Science
at the University of Cape Town

Abstract

We review a cluster model for even-even nuclei and derive a new relation between the excitation energies and the electric quadrupole transition strengths of these nuclei. A novel method for determining the likely cluster-core decompositions of a given nucleus is described, and is tested by comparing theoretical cluster model spectra with their experimental counterparts for a representative set of Yb isotopes. A further method, based on least squares fits to spectra, is also examined.

Contents

Acknowledgements

I would like to thank my supervisor, Prof. S. M. Perez, for his patience, unwavering support and sense of humour.

I am grateful to my colleagues at Necsa for their interest and advice.

Thanks to all my friends for help with the technicalities, good ideas and the odd drink when required.

To Brent, thank you for your motivation, time and continual encouragement.

Finally, I am grateful to the National Research Foundation (NRF) for their financial support during 2002 and 2003.

Chapter 1

Introduction

In this section the most common models of nuclear structure, the shell model and the vibrational and rotational models, are briefly reviewed. The cluster model is introduced and its basic properties described. Chapter 2 contains a more detailed description of the cluster model, beginning with the important issues of how to determine the cluster-core decompositions of a given nucleus, what form to take for the cluster-core potential and what quantum numbers to assign to the cluster-core relative motion. Methods for generating cluster model spectra are next discussed and expressions for the electric dipole B(E1) and quadrupole B(E2) transition strengths derived. In Chapter 3 an investigation of the relation between cluster model excitation energies and electric quadrupole strengths is undertaken, and results compared with experiment. A technique for determining cluster-core decompositions from these strengths is then derived, and Chapter 4 provides a full implementation of the cluster model for selected isotopes of Yb, comparing cluster model generated spectra to experimental spectra. Chapter 5 examines the feasibility of determining cluster-core decompositions directly from fits to experimental energy level spectra, and Chapter 6 summarises the conclusions reached in this thesis.

1.1 The Shell Model

In the extreme form of this model (the single particle shell model) the nucleons in the nucleus move independently in a common potential. The nucleus is visualized as consisting of filled shells that contain the maximum number of neutrons and protons permitted by the Pauli exclusion principle, and

unfilled shells containing the remaining number of neutrons and protons.

Strong experimental evidence supports the point of view that when a nucleus contains 2, 8, 20, 50, 82, or 126 protons or neutrons, a shell closure exists. That is, the energy separation between levels belonging to different major shells is significantly larger than the energy separations between the levels within a shell. Consequently it is more difficult to excite one of these nuclei. These nuclei are known as magic nuclei and, in its earliest applications, the main objective of the shell model was to reproduce these magic numbers.

Closed shell nuclei are thus particularly stable, and the pairwise filling of the shells makes no contribution to the total spin and electromagnetic moments. Such nuclei correspond to an inert core and the properties of a closed-shell + 1 (or closed-shell − 1) nucleon nucleus are characterized by those of the valence nucleon (or hole). Similarly, for closed-shell + 2 nucleon nuclei the two valence nucleons are largely responsible for the properties of the low-lying states, although it should be noted that the valence nucleon - valence nucleon two-body interaction needs to be introduced, since its matrix elements are typically comparable to sub-shell spacings.

To determine how the nucleons fill the various single particle levels of the nucleus (i.e. the spectrum of quantum states into which any one nucleon can enter) it is necessary to specify the common potential. The potential most often used to describe the nucleus is the Woods-Saxon potential given by:

$$V_0(r) = -V_0 f(r) = \frac{-V_0}{1 + \exp(r - R)/a} \tag{1.1}$$

This potential has an experimental basis obtained by fitting data from closed-shell + 1 and closed-shell - 1 nucleon nuclei [1] and from nucleon-nucleus scattering [2]. Its parameters have typical values $V_0 \sim 50$ MeV, $R = r_0 A^{1/3}$ fm where $r_0 \sim 1.3$ fm, and $a \sim 0.75$ fm.

In order to obtain calculated single particle energy spectra which agree with experimental spectra, it is necessary to add a spin-orbit interaction term to the potential. This term takes account of the fact that nucleons have an intrinsic spin 1/2 which can interact with the orbital angular momentum. Thus, each previous state corresponding to an orbital angular momentum quantum number l is split into 2 states: $j = l + 1/2$ and $j = l - 1/2$. This

interaction is often given the surface-peaked functional form

$$V_{\mathrm{l}}(r) = -V_{\mathrm{l}}\left(\frac{\hbar}{m_\pi c}\right)^2 \frac{1}{r}\frac{df(r)}{dr}\mathbf{l}\cdot\mathbf{s} \tag{1.2}$$

with l and s the orbital and spin angular momentum operators respectively, $f(r)$ the Woods-Saxon form defined above, and $V_{\mathrm{l}} \sim 10$ MeV. A single particle potential described by Eqs.(1.1) and (1.2) then results in the reproduction of the magic numbers [3] as well as a reasonably good description of the properties of single particle and single hole nuclei [1, 3].

Further away from closed shells the main shortfall of the shell model is that it quickly becomes difficult to apply in practice, with the number of configurations that have to be taken into account increasing rapidly as the number of nucleons outside the closed shell increases.

1.2 The Collective Models of even-even Nuclei

Away from closed shells nuclei exhibit large quadrupole moments, indicative of the coherent motion of a large number of valence nucleons, which is difficult to account for using a shell model. It is then more profitable to use models in which collective motion is intrinsic, such as the vibrational or rotational models developed by Bohr, Mottelson and Rainwater. For even-even nuclei, as one moves away from closed shells the nucleus becomes more easily deformable about its spherical equilibrium shape, and low-lying vibrational modes become possible. The energies of these vibrational states increase with increasing multipolarity L, and for an incompressible nucleus ($L = 0$ forbidden) with its centre of mass at rest ($L = 1$ forbidden), the lowest mode corresponds to $L = 2$. The quadrupole phonons associated with this mode have characteristic energy quanta $\hbar\omega$, and nuclear states are then equispaced and associated with zero-phonon, one-phonon, two-phonon states etc. (Figure 1.1)

Further away from a closed shell, as more nucleons are added, permanent distortion of the nucleus may occur, with an ellipsoid being the simplest such deformed shape. Now there is the possibility for rotation of the nucleus about an axis which is not the axis of symmetry. This gives rise to rotational modes (Figure 1.2) with energies lower than those of the corresponding vibrational modes. When certain hypotheses about axial and

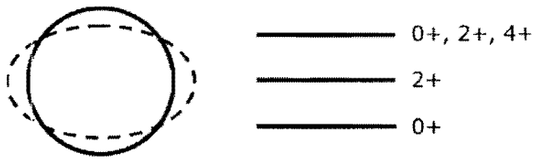

Figure 1.1: *Nuclear vibration leading to low-lying vibrational states*

equatorial symmetries are made, the rotational model then yields a lowest energy (ground state) band with spin-parity $J^\pi = L^\pi = 0^+, 2^+, 4^+, \ldots$ having characteristic rotational energies $E_J^* \propto J(J+1)$.

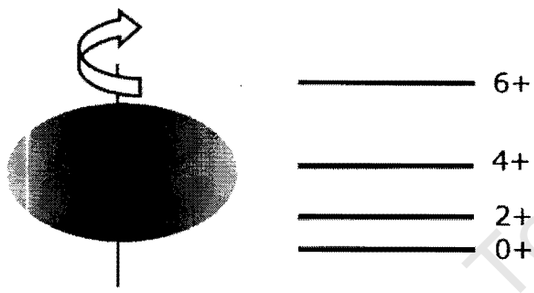

Figure 1.2: *Nuclear deformation leading to rotational states*

It is interesting to note that as nuclei move away from closed shells, their energy spectra change from single particle excitations in a spherical potential well, through vibrational modes, up to rotational spectra furthest away from a closed shell. This 'evolution' then occurs in reverse as the nuclear mass is increased further, approaching the next closed shell.

1.3 The Cluster Model

In the cluster model the nucleus is represented by a core and cluster which interact via a common potential. The nuclear many-body problem is reduced to a 2-body problem, which can then be separated into a centre-of-mass plus relative motion system, with the physics contained in the latter.

The cluster model can support a variety of nuclear behaviour ranging from uncorrelated motion (as in the single particle shell model) to highly corre-

lated motion (as in a collective model). This is achieved by the choice of cluster - it could be chosen as one nucleon, or as equal in size to the core.

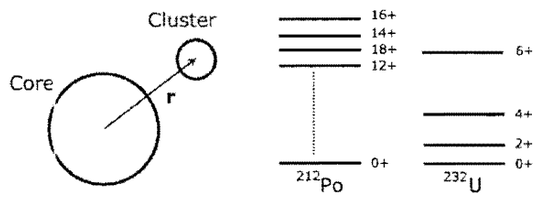

Figure 1.3: *Schematic diagram of cluster and core, and spectra generated with the cluster model*

For even-even nuclei, on which this thesis will concentrate, the characteristic $J^\pi = L^\pi = 0^+, 2^+, 4^+, \ldots$ states of the 'ground state band' is achieved because the band is described by an even value of the global quantum number (described in Chapter 2) $G = 2n + L$. Since the node number n is integral, only even values of the orbital angular momentum L are then allowed. However, the pattern of the model spectrum is not fixed as in the vibrational or rotational cases above, but can vary significantly depending on the cluster size. In extreme cases, such as for ^{212}Po with an α-particle as cluster, the model spectrum is compressed and even inverted for high L [4], whereas for ^{232}U with ^{24}Ne as the cluster, the spectrum is quasi-rotational [5] (Figure 1.3). Similarly odd values of G generate bands with $J^\pi = 1^-, 3^-, 5^-, \ldots$ with properties corresponding to those observed for low-lying negative parity bands in heavy nuclei [6].

Chapter 2

Overview of the Cluster Model

The most important ingredients in any application of the cluster model are a) choosing an appropriate cluster-core configuration, b) choosing a form of the potential for the cluster-core interaction, and c) specifying the quantum numbers of the cluster-core relative motion.

2.1 Choice of Cluster and Core

Fundamental to applying the cluster model to a given nucleus of total mass A and total charge Z is the choice of cluster and core, i.e. the split of the given nucleus into the masses A_2 and A_1, and corresponding charges Z_2 and Z_1, of cluster and core respectively.

Nuclear reaction and decay data supply information on possible cluster-core decompositions. In various light nuclei, the presence of an α cluster may be indicated by strong selective excitation in α transfer reactions and by the existence of α widths in resonant states above threshold [7, 8]. The existence of α and exotic decay in heavy nuclei suggests that an α or heavier particle may be present as a cluster in the parent nucleus.

Buck et al [9] have used an α cluster and a doubly magic core to model a number of light and heavy nuclei (^{20}Ne, ^{44}Ti, ^{94}Mo, ^{212}Po). The doubly magic cluster and core involved here are extremely stable against internal break-up and are a likely choice for the cluster-core decomposition of the parent nucleus. This approach successfully reproduced spectra, α-decay

half-lives and reduced E2 (quadrupole) transition strengths, thereby reinforcing the hypothesis that α clusters are present in various light and heavy nuclei.

Resonances in the scattering of some light heavy ions (^{12}C,^{16} O), as well as the phenomenon of exotic decay in heavy nuclei, have given reason to suspect, in nuclei, the existence of clusters heavier than α clusters. A cluster model employing exotic clusters was implemented by Buck et al [5] in an analogous manner to that using α clusters, by scaling certain parameters of the α cluster model. So, for an exotic cluster of mass A_c, the potential strengths and orbit G-value (see Section 2.3) were scaled with A_c. Using this approach, they found [5] that the exotic decay half-lives calculated in the same way as α decay half-lives fall within a factor of 2-3 of the experimentally measured decay half-lives for all known even-even to even-even exotic decays. Further, when spectra for nuclei having exotic decays to a ^{208}Pb ground state are generated using an exotic cluster model they show excellent agreement with experimental spectra, including compression of the higher L-values in the spectrum relative to a pure rotational spectrum, and lowering of 4^+ excitation energies with increasing cluster mass (i.e. increasing deformation).

Table 2.1. Comparison of theoretical, B(E2 $\downarrow)^T$, and experimental, B(E2 $\downarrow)^E$ transition strengths using an exotic cluster model. Taken from [5].

Decay	B(E2 $\downarrow)^T$ (W.u.)	B(E2 $\downarrow)^E$ (W.u.)
^{222}Ra($2^+ \rightarrow 0^+$)	107	111±9
^{228}Th($2^+ \rightarrow 0^+$)	170	167±6
^{232}U ($2^+ \rightarrow 0^+$)	250	241±21
^{236}Pu($2^+ \rightarrow 0^+$)	360	-
^{228}Th($2^+ \rightarrow 0^+$)	170	167±6
^{228}Th($4^+ \rightarrow 2^+$)	243	242±9
^{228}Th($6^+ \rightarrow 4^+$)	267	-
^{228}Th($8^+ \rightarrow 6^+$)	278	-

Finally, in [5], Buck et al showed that an exotic cluster model applied to nuclei in the Actinide region reproduces the observed pattern of large B(E2) strengths in the ground state bands, for both $L \rightarrow L-2$ transitions within

a single nucleus and for $2^+ \rightarrow 0^+$ transitions for a range of nuclei - see Table 2.1. A noticeable trend is the jump in B(E2) values from one isotope set to another, which can be correlated with changes in the cluster charge. This agreement between cluster model predictions and experimental observations supports the hypothesis that exotic clusters are present in the parent nuclei. We note here that throughout this thesis we use the notation

$$\mathrm{B(E2)} = \mathrm{B(E2\downarrow)} = \mathrm{B(E2:}\ 2^+ \rightarrow 0^+)$$

Further investigations were undertaken by Buck et al in [6] into all Actinide nuclei which can be described as binary systems comprising a Pb core and a cluster observed in exotic decay. In this investigation a single cluster-core potential, labeled $T1$, with fixed parameter values was used throughout. Only the nuclear potential radius, R, was fitted to each individual binary system. The overall agreement with experimental spectra was surprisingly good, and could be improved by systematically changing the erstwhile fixed potential. One other clear opportunity for improvement was that the 0^+ to 2^+ and 1^- to 3^- energy gaps tended to be underestimated, possibly indicating the need to refine the cluster-core potential in the region $r = 0$.

Up to this time, applications of the cluster model had been limited to sections of the Periodic Table where there was external evidence of clustering such as α or exotic decay in heavy nuclei, or where the greater stability of a nearby doubly closed shell indicated a good candidate for a core. In an attempt to make applications of the cluster model more universal, other methods for determining cluster-core combinations were considered. This led [10] to the maximum stability criterion according to which a nucleus (A, Z) should be split into even-even cores (A_1, Z_1) and clusters (A_2, Z_2), such that the value of the function $D = [B_A(1) - B_L(1)] + [B_A(2) - B_L(2)]$ is maximised, where B_A is an actual binding energy and B_L is a liquid drop binding energy given by

$$B_L = a_v A - a_s A^{2/3} - a_c \frac{Z^2}{A^{1/3}} - a_a \frac{(A-2Z)^2}{A} + \delta$$

where $a_v = 15.56$, $a_s = 17.23$, $a_c = 0.697$, $a_a = 23.285$ and $\delta = 12/\sqrt{A}$ are empirically determined constants, with all values in MeV. [11]

The numbers (1) and (2) in the expression for D above refer to the core and cluster chosen. A local maximum of D thus indicates a combination

of core and cluster whose internal stability is greater than that expected on average, and which, by hypothesis, are then good candidates for the core and cluster to be used in a cluster model. As it stands the method is difficult to apply to a given parent nucleus (A, Z) since D remains a function of two independent variables, say (A_2, Z_2), after the conditions $A_1 = A - A_2$ and $Z_1 = Z - Z_2$ have been applied. Thus in their paper [10], Buck et al introduce a method of utilising the maximum stability criterion involving only the variable Z_2. This is achieved by imposing the no-dipole constraint: due to the observed weakness of electric dipole transitions in heavy nuclei it is assumed that the charge and mass of the nucleus are distributed in the same proportions between the core and cluster. This implies satisfying the constraint (see Section 2.4.1):

$$\frac{Z_1}{A_1} = \frac{Z_2}{A_2} = \frac{Z}{A}$$

To implement the above constraint it is necessary to consider nuclear states as a superposition of several possible cluster-core configurations, as the constraint cannot in general be satisfied by a single choice of even-even core and cluster. The method thus entails choosing an arbitrary average value of the cluster charge $< Z_2 >$, and determining the corresponding cluster mass $< A_2 >$ from the no-dipole relation. Even-even clusters with values of Z_2 and A_2 bracketing $< Z_2 >$ and $< A_2 >$ respectively are selected next and each is allocated a probability weighting such that the weighted combination of these even-even clusters yields the average values $< Z_2 >, < A_2 >$ [10]. Mixtures of cluster-core decompositions where the clusters (and cores) are of similar mass and charge thus arise, consistent with the observation of more than one type of exotic decay of a given nucleus e.g. the Ne and Mg decay of ^{234}U. A typical D-plot for the heavy nucleus ^{228}Th is shown in Figure 2.1, where the dashed line is the full calculation, and the solid line a smoothed curve obtained by applying a Fourier-based filtering process. The peak at $< Z_2 > \sim 8$ corresponds to the exotic clustering discussed above, and the peak at $< Z_2 > \sim 36$ has been tied in with superdeformation [10].

The most recent development in deducing cluster-core decompositions by Buck, Merchant, McBride and Perez [12] is described in detail in Chapter 3.

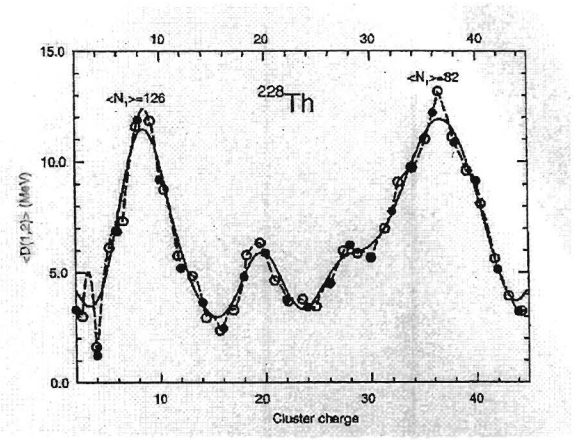

Figure 2.1: *D-plot for* ^{228}Th

2.2 Cluster-Core Interaction

The cluster is assumed to interact with the core by means of a local, central potential $V_T(r)$, which comprises nuclear $V_N(r)$, Coulomb $V_C(r)$, and centrifugal terms. The general form of the potential is:

$$V_T(r) = V_N(r) + V_C(r) + \frac{\hbar^2 L(L+1)}{2\mu r^2} \tag{2.1}$$

In the work of Buck et al, a variety of nuclear cluster-core potentials have been used. These range from a simple square-well potential to a modification of the frequently used Woods-Saxon (SW) potential. In choosing a nuclear potential, a simple geometric form is assumed, and the potential parameters are then refined by fitting to experimental data such as energy levels or elastic scattering data. Batty et al [13] showed that a Woods-Saxon form of the nuclear potential poorly reproduces experimental cross sections for α elastic scattering, and much improved fits were obtained by Michel et al for $^{16}\mathrm{O}(\alpha,\alpha)^{16}\mathrm{O}$ [14] and $^{40}\mathrm{Ca}(\alpha,\alpha)^{40}\mathrm{Ca}$ [15] using a $(\mathrm{SW})^2$ form of the α-core potential. Cluster model studies of bound and quasibound α-cluster states, as well as of low energy α elastic scattering for a number of nuclei [16, 17] have shown that a mixed $(SW)+(SW)^3$ Woods-Saxon form of the cluster-core nuclear potential also produced good fits to experimental elastic scattering data as well as to experimental spectra and decay half-lives. This potential is given by

$$V_N(r) = -V_0\left[\frac{x}{1+\exp[(r-R)/a]} + \frac{1-x}{\{1+\exp[(r-R)/3a]\}^3}\right] \quad (2.2)$$

$$= -V_0 f(r,x,a,R) \quad (2.3)$$

with V_0 the potential depth, R the potential radius, a the diffuseness, and x a mixture parameter.

In early cluster model applications using this form of the cluster-core potential a and x were held fixed at values $a \sim 0.75$ fm and $x \sim 0.35$, and V_0 and R optimised to obtain the best agreement with available data on elastic scattering, nuclear spectra, and decay half-lives. For α-clustering it was found that the optimum $r = 0$ value of the potential $V_N(0)$ increased systematically with increasing core mass so that e.g. $V_N(0) = 164$, 193 and 219 MeV for the nuclei ^{20}Ne, ^{44}Ti, and ^{212}Po respectively [18]. Further, for α and exotic clustering in heavy nuclei the optimum $V_N(0)$ value scaled approximately with cluster mass.

In their paper [18], Buck et al set out to determine a general form of the potential applicable to any cluster model environment and having similar default parameter values for widely different clusters and cores. They imposed the following three conditions on the potential:

1. The potential should be symmetric in core (A_1) and cluster (A_2) masses,

2. For fixed cluster mass (A_2), the potential depth at the origin, $V_N(0)$, should increase with increasing core mass (A_1), until saturation is reached for $A_1 \gg A_2$,

3. For $A_1 \gg A_2$, $V_N(0)$ should be proportional to the cluster mass, A_2.

Point 1. is required on the general physical grounds that the potential should be invariant in the interchange of core and cluster. Points 2. and 3. follow from the results of the early cluster model applications described above.

The nuclear potential chosen to satisfy the above constraints has the form for $A \gg 1$

$$V_N(r) = -\left(\frac{A_1 A_2}{A}\right) U_0 \frac{f(r,x,a,R)}{f(0,x,a,R)} \quad (2.4)$$

with $U_0 = 54$ MeV, $x = 0.33$, $a = 0.73$ fm, and f defined in Eqs.(2.2) and (2.3).

Besides the nuclear part of the potential, $V_N(r)$, the Coulomb contribution $V_C(r)$ must also be included. This is taken to be the potential between a uniformly charged spherical core of charge Z_1 and a point cluster of charge Z_2, given by:

$$V_C(r) = \frac{Z_1 Z_2 e^2}{r} \qquad \text{for } r \geq R_C \tag{2.5}$$

$$= \frac{Z_1 Z_2 e^2}{2R_C}\left[3 - \left(\frac{r}{R_C}\right)^2\right] \qquad \text{for } r \leq R_C \tag{2.6}$$

where R_C is the radius of the spherical core. In cluster model calculations this is set to R, the nuclear potential radius, in order to reduce the number of adjustable parameters.

This mass-symmetric form of the potential has undergone various tests to check its validity. [18]

- For α clustering the values of $V_N(0)$ calculated from the mass-symmetric potential agree well with those calculated from the optimised α-core potential of the earlier form of Eq.(2.2).

- Excitation energies and B(E2) values calculated for medium ($\alpha + {}^{44}$Ti) and heavy ($\alpha + {}^{208}$Pb) mass systems, are in agreement with experimental values, on a par with those obtained using the optimised nuclear potential of the earlier form of Eq.(2.2).

- The spectrum, half-life and B(E2) values of ^{222}Ra, modelled as ^{14}C+^{208}Pb system interacting via the mass symmetric potential show good agreement with experiment.

- The mass symmetric form of the nuclear potential also mimics well a form previously used [19] to reproduce $\alpha - \alpha$ scattering, and its use in a cluster model treatment of ^{24}Mg (which shows strong evidence of ^{12}C +^{12} C clustering [20]) yields good agreement with experiment for energy levels and B(E2) values.

It should be noted that most of the tests performed by Buck et al rely on spectra and B(E2) values, due to the fact that elastic scattering requires

an additional imaginary part of the cluster-core potential, which introduces further parameters. Comparison with elastic scattering data may well lead to improvements of the cluster-core potential. However, the above simple mass symmetric form has been shown to be quite successful, and shall be used in all further calculation in this thesis.

2.3 Expressions for Cluster Model Energies

Many tests of the validity of nuclear models are performed by using the potential defined by the model to generate energy spectra, which are then compared with experimentally observed spectra. This is no less the case for applications of the cluster model, and two approaches to generating these spectra are shown below. The sole criterion for applying these approaches to a given nuclear model is that one must have a well-defined potential.

The energy of relative motion between the cluster and core of a given nucleus, where the potential function is known, can be determined by solving the radial Schrödinger equation, which takes the following form:

$$\frac{-\hbar^2}{2\mu}\frac{d^2\psi_{nL}(r)}{dr^2} + \left[V_N(r) + V_C(r) + \frac{\hbar^2 L(L+1)}{2\mu r^2}\right]\psi_{nL}(r) = E_{nL}\psi_{nL}(r) \quad (2.7)$$

where E_{nL} is the energy of relative motion of core and cluster in a state with radial and angular momentum quantum numbers n and L respectively.

As an alternative method of generating nuclear spectra, we can use a semi-classical integral form of the Schrödinger equation known as the Bohr-Sommerfeld quantization rule. This has the form:

$$\begin{aligned}\int_{r_1}^{r_2} dr \sqrt{\frac{2\mu}{\hbar^2}\left[E_{nL} - V_N(r) - V_C(r) - \frac{\hbar^2 L(L+1)}{2\mu r^2}\right]} &= (2n+1)\frac{\pi}{2} \\ &= (G - L + 1)\frac{\pi}{2}\end{aligned} \quad (2.8)$$

where r_1 and r_2 are the innermost classical turning points.

The global quantum number G (or equivalently the value of n for $L = 0$) is best described in a pure harmonic oscillator environment. On one hand the nucleons can be thought of as occupying the oscillator states of a single nucleus, and the total number of oscillator quanta for the nucleus can thus

be found. On the other hand one can apportion the core nucleons to the lowest available states of the core, and the remainder to the lowest available states of the cluster. The remaining quanta are then available for the relative motion of core and cluster, and they define the principal quantum number G of this motion. For example, consider the partitioning given by

$$^{232}_{92}\mathrm{U}^{140} \rightarrow ^{208}_{82}\mathrm{Pb}^{126} + ^{24}_{10}\mathrm{Ne}^{14}$$

The lowest states of ^{208}Pb are common both to the LHS and RHS. In a pure oscillator model the 10 remaining protons in ^{232}U are in $g = 5$ state and the 14 remaining neutrons in $g = 6$ state resulting in a total number of oscillator quanta $\Sigma_i g_i = 134$ for these nucleons. (Here g is the principal quantum number for the harmonic oscillator potential). For the RHS the 10 protons in ^{24}Ne can be apportioned to the 0s, 0p, (1s0d) orbits of this nucleus, and similarly for the 14 neutrons. This results in $\Sigma_i g_i = 28$ oscillator quanta for ^{24}Ne. Thus $G = 134 - 28 = 106$ quanta are available for the core-cluster relative motion. This application of the Wildermuth condition can be viewed as giving a reasonable guess at G, and calculations in the rare-Earth and Actinide regions by Buck et al have successfully used the simple prescription $G = gA_c$ where A_c is the cluster mass, and $g = 4$ and 5 in the rare-Earth and Actinide regions respectively. In a harmonic oscillator the states with $J^\pi = L^\pi = 0^+, 2^+, 4^+, \ldots G^+$ would all be degenerate. A potential such as the mass-symmetric one of Eq.(2.4) results in the degeneracy being removed and the appearance of a band of levels with $J^\pi = 0^+, 2^+, 4^+, \ldots G^+$.

2.4 Multipole Transitions

A significant part of this thesis centres around dipole B(E1) and quadrupole B(E2) transition strengths, and a derivation of these transition strengths now follows. The interaction between the charge distribution of a nucleus and an electromagnetic field gives rise to radiation as well as to a B(Ex) value corresponding to the transition strength between an initial state and final state of the charge distribution of a nucleus.

The operator inducing electric transitions between an initial state Ψ_i and final state Ψ_f of the charge distribution, giving rise to the emission of a photon of angular momentum lm is given by:

$$H' = \sum_i q_i r_i^l Y_{lm}^*(\theta_i, \phi_i) \tag{2.9}$$

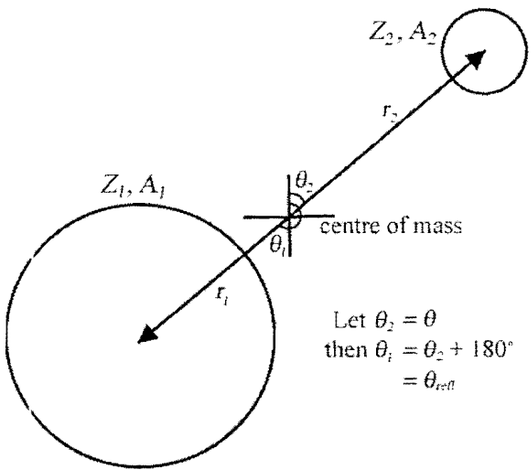

Figure 2.2: *Geometry of the cluster model*

where q_i is the charge of the i^{th} particle of the charge distribution, and r_i, θ_i, ϕ_i are the coordinates corresponding to its position.
The transition strength is related to the probability of this process occurring and is given as $| < \Psi_f | H' | \Psi_i > |^2$.

2.4.1 Dipole Transition Strengths (B(E1))

The dipole transition strength between the 1^- and 0^+ band heads of the corresponding negative and positive parity bands is given by:

$$B(E1) = | < \Psi_{00} | \sum_i q_i r_i Y^*_{1m}(\theta_i, \phi_i) | \Psi_{1m} > |^2 \tag{2.10}$$

which, in a cluster model reduces to (see Figure 2.2)

$$B(E1) = | < \Psi_{00}(\vec{r}) | Z_1 r_1 Y^*_{1m}(\theta_1, \phi_1) + Z_2 r_2 Y^*_{1m}(\theta_2, \phi_2) | \Psi_{1m}(\vec{r}) > |^2$$

where $\vec{r}$ is the cluster-core separation vector.
Splitting the wavefunctions into their radial and angular components

$$\Psi_{lm}(\vec{r}) = \frac{\psi_l(r)}{r} Y_{lm}(\theta, \phi)$$

and substituting $Y_{00}(\theta, \phi) = \frac{1}{\sqrt{4\pi}}$, $\theta_2, \phi_2 = \theta, \phi$, and $\theta_1, \phi_1 = \theta_{refl}, \phi_{refl}$, results in:

$$B(E1) = |\frac{1}{\sqrt{4\pi}} < \frac{\psi_0(r)}{r}|Z_1 r_1 Y^*_{1m}(\theta_{refl}, \phi_{refl}) + Z_2 r_2 Y^*_{1m}(\theta, \phi)|\frac{\psi_1(r)}{r} Y_{1m}(\theta, \phi) > |^2$$

Now inserting the following expressions into this equation

$$Y_{lm}(\theta_{refl}, \phi_{refl}) = (-1)^l Y_{lm}(\theta, \phi)$$

$$r_1 = \frac{A_2}{A} r \qquad r_2 = \frac{A_1}{A} r$$

leads to

$$B(E1) = \frac{1}{4\pi}| < \frac{\psi_0(r)}{r}|\left(\frac{Z_2 A_1 - Z_1 A_2}{A}\right) r Y^*_{1m}(\theta, \phi)|\frac{\psi_1(r)}{r} Y_{1m}(\theta, \phi) > |^2$$

Integration over the angles, using

$$\int_0^{2\pi} \int_0^{\pi} Y^*_{1m}(\theta, \phi) Y_{1m}(\theta, \phi) \sin\theta d\theta d\phi = 1$$

results in the expression for the dipole transition strength

$$B(E1) = \frac{1}{4\pi}\left[\left(\frac{Z_2 A_1 - Z_1 A_2}{A}\right) \int \psi_0(r)\psi_1(r) r dr\right]^2 \tag{2.11}$$

Now, if the dipole transition strength B(E1) vanishes, this implies that

$$Z_2 A_1 - Z_1 A_2 = 0$$

thus

$$\frac{Z_1}{A_1} = \frac{Z_2}{A_2}$$

and since

$$Z_2 = Z - Z_1 \qquad A_2 = A - A_1$$

it follows that

$$\frac{Z_1}{A_1} = \frac{Z}{A}$$

which results in the no-dipole condition:

$$\frac{Z_1}{A_1} = \frac{Z_2}{A_2} = \frac{Z}{A} \tag{2.12}$$

2.4.2 Quadrupole Transition Strengths (B(E2))

A similar derivation to that above applies to the electric quadrupole transition strength, involving the emission of a photon of quadrupole radiation due to a transition between an $l = 2$ and $l = 0$ state.

Thus (2.10) becomes

$$B(E2) = |<\Psi_{00}|\sum_i q_i r_i^2 Y_{2m}^*(\theta_i, \phi_i)|\Psi_{2m}>|^2 \tag{2.13}$$

For a cluster model, following through the same steps as for the dipole transition strength we obtain:

$$B(E2) = \frac{1}{4\pi}|<\frac{\psi_0(r)}{r}|Z_1\left(\frac{A_2 r}{A}\right)^2 Y_{2m}^*(\theta,\phi)+Z_2\left(\frac{A_1 r}{A}\right)^2 Y_{2m}^*(\theta,\phi)|\frac{\psi_2(r)}{r}Y_{2m}(\theta,\phi)>|^2$$

We now implement the no-dipole condition from Eq.(2.12) - in the following form:

$$\frac{Z_1}{Z} = \frac{A_1}{A} \qquad \frac{Z_2}{Z} = \frac{A_2}{A}$$

so that

$$\begin{aligned} B(E2) &= \frac{1}{4\pi}|<\frac{\psi_0(r)}{r}|Z_1\left(\frac{Z_2}{Z}\right)\frac{A_2}{A}r^2 Y_{2m}^*(\theta,\phi) \\ &+ Z_2\left(\frac{Z_1}{Z}\right)\frac{A_1}{A}r^2 Y_{2m}^*(\theta,\phi)|\frac{\psi_2(r)}{r}Y_{2m}(\theta,\phi)>|^2 \end{aligned}$$

and the expression for the electric quadrupole transition strength reduces to

$$B(E2) = \frac{1}{4\pi}\left[\frac{Z_1 Z_2}{Z}\int \psi_0(r) r^2 \psi_2(r) dr\right]^2 \tag{2.14}$$

Chapter 3

Relation between B(E2) values and Excitation Energies

A correlation between the observed electric quadrupole transition strength B(E2) = B(E2: $2^+ \rightarrow 0^+$) for the lowest 2^+ state of a non-magic nucleus and the corresponding excitation energy $(E_2 - E_0)$ has been known to exist for some time and was first pointed out by Grodzins [21] using a functional form suggested by the vibrational and rotational models (VRM) of Bohr and Mottelson [22]. In this treatment, the B(E2) value is dependent on the nuclear charge, Z, the nuclear mass, A, and the corresponding excitation energy. It has the following functional form:

$$B(E2) = \frac{aZ^2}{(E_2 - E_0)A^{1/3}} e^2\mathrm{fm}^4 \tag{3.1}$$

where a is a proportionality constant with a value ranging between 14 (for the vibrational model) and 6 (for the rotational model), with a best-fit value of 1.37 from a recent fit [23] to a large body of data. Using this functional form, the model produces good agreement between the B(E2) value deduced from the excitation energy of the first 2^+ state and the corresponding experimental B(E2) values.

3.1 Derivation of B(E2) - Energies Relation

In this chapter we use a binary cluster model of the nucleus to derive and test a new relation between quadrupole transition strengths and excitation energies [12].

The binary cluster model has been described in detail in Chapter 2, and we will begin the derivation of the new relation by considering two states, ψ_L and ψ_l of angular momenta L and l respectively, and corresponding energies E_L and E_l. These two states are members of a ground state band of angular momenta states: $L^\pi = 0^+, 2^+, 4^+ \ldots$, and each state is a solution of the radial Schrödinger equation, as shown below.

$$\begin{aligned}\left[\frac{-\hbar^2}{2\mu}\frac{d^2}{dr^2} + V_N(r) + V_C(r) + \frac{\hbar^2 L(L+1)}{2\mu r^2}\right]\psi_L &= E_L\psi_L \\ \left[\frac{-\hbar^2}{2\mu}\frac{d^2}{dr^2} + V_N(r) + V_C(r) + \frac{\hbar^2 l(l+1)}{2\mu r^2}\right]\psi_l &= E_l\psi_l\end{aligned}$$

Premultiplying the first equation by ψ_l, the second by $-\psi_L$ and adding the results:

$$\psi_L\frac{d^2\psi_l}{dr^2} - \psi_l\frac{d^2\psi_L}{dr^2} - \frac{1}{r^2}\{L(L+1) - l(l+1)\}\psi_L\psi_l = \frac{2\mu}{\hbar^2}\{E_L - E_l\}\psi_L\psi_l$$

so that

$$r^2\frac{d}{dr}\left[\psi_L\frac{d\psi_l}{dr} - \psi_l\frac{d\psi_L}{dr}\right] + \{L(L+1) - l(l+1)\}\psi_L\psi_l = \frac{2\mu}{\hbar^2}\{E_L - E_l\}r^2\psi_L\psi_l$$

If we integrate $\int_0^\infty dr$ and take note of the following:

- The wavefunctions ψ are normalized to unity and $\psi(0) = \psi(\infty) = 0$
- In [24], it is shown that the radial multinodal wavefunctions of the low-lying angular momentum states in the same band are closely similar near their peak in the surface region, and thus $\psi_L \sim \psi_l$ and $\frac{d\psi_L}{dr} \sim \frac{d\psi_l}{dr}$

This results in the following relation:

$$\{L(L+1) - l(l+1)\} \sim \frac{2\mu}{\hbar^2}(E_L - E_l)\int_0^\infty r^2\psi_L\psi_l dr \qquad (3.2)$$

Now, in section 2.4.2, Eq.(2.14), an expression for the quadrupole transition strength was derived from a cluster model treatment as:

$$B(E2) = \frac{1}{4\pi}\left[\frac{Z_1 Z_2}{Z}\int_0^\infty \psi_0(r) r^2 \psi_2(r) dr\right]^2$$

Substituting this into the above relation and applying the no-dipole condition from Eq.(2.12) results in

$$B(E2) \approx \frac{1}{4\pi}\left[\frac{\hbar^2}{2}\left\{\frac{L(L+1)-l(l+1)}{E_L - E_l}\right\}\frac{Z}{A}\right]^2 e^2\mathrm{fm}^4 \tag{3.3}$$

where $\hbar^2 = 41.8$ when energies are expressed in MeV throughout.

Some noteworthy points regarding Eq.(3.3) are:

1. The result is independent of the cluster-core potential, $V(r)$, as long as all members of the chosen angular momentum band have the same form of this potential.

2. The result critically depends on two cluster model ingredients i.e. that the no-dipole condition of Eq.(2.12) applies, and that the low angular momentum multinodal members of a band have similar surface-peaked radial wave functions.

3.2 Cluster Model Calculations of B(E2) values

In our calculations of B(E2) values from Eq.(3.3), we follow a similar path to Raman et al [23] by including an overall normalization constant, b. We thus use

$$B(E2) \approx \frac{b}{4\pi}\left[\frac{\hbar^2}{2}\left\{\frac{L(L+1)-l(l+1)}{E_L - E_l}\right\}\frac{Z}{A}\right]^2 e^2\mathrm{fm}^4 \tag{3.4}$$

The above result should hold for all values of L and l within the same angular momentum band, perhaps with different values of b for each pair. Because the lowest angular momentum states constitute the most comprehensive datasets it would seem sensible to use $L = 2$ and $l = 0$ in calculations of the B(E2) values. However, it has been found that in applications of the cluster model, the $l = 0$ angular momentum state is often underbound with respect to the rest of the spectrum, leading to the $L = 2$ to $l = 0$ excitation

energy being less well reproduced in the model than all other transitions. Trials have shown that using these angular momentum values to test the above relation leads to inferior results, and henceforth we have used angular momentum values $L = 4$ and $l = 2$.

In Figure 3.1 B(E2) values obtained from Eq.(3.4) are compared with experimentally determined B(E2) values. As discussed above, for this plot we use $L = 4$, $l = 2$ and a fitted value of $b = 0.35$. Table 3.1 shows the overall level of the fit of the calculated B(E2) values to observed values, and compares it to the corresponding level of fit using the VRM model of Eq.(3.1) with $a = 1.37$ [23]. (See also Appendix A for a comparison of individual cases). We have left out all singly and doubly magic nuclei and have plotted them separately in Figure 3.2. Table 3.2 shows the overall level of fit for the magic nuclei.

Table 3.1. Non-magic nuclei: percentage of B(E2)'s for which the theoretical value is within a factor f of the experimental value.

Factor f	VRM	Cluster Model
2.00	93.0%	88.3%
1.50	70.6%	69.6%
1.25	43.0%	43.5%

Table 3.2. Magic nuclei: Percentage of B(E2)'s for which the theoretical value is within a factor f of the experimental value.

Factor f	VRM	Cluster Model
2.00	75.5%	34.0%
1.50	54.7%	26.4%
1.25	30.2%	22.6%

For non-magic nuclei the results are in good agreement with experiment, with the B(E2) values of only a few nuclei being more than a factor of 2 different to the experimentally determined values. The cluster model values give a very similar level of fit to experiment to the Bohr and Mottelson vibrational/rotational (VRM) values for the non-magic nuclei, despite the very different functional forms obtained for the two cases. For magic nuclei,

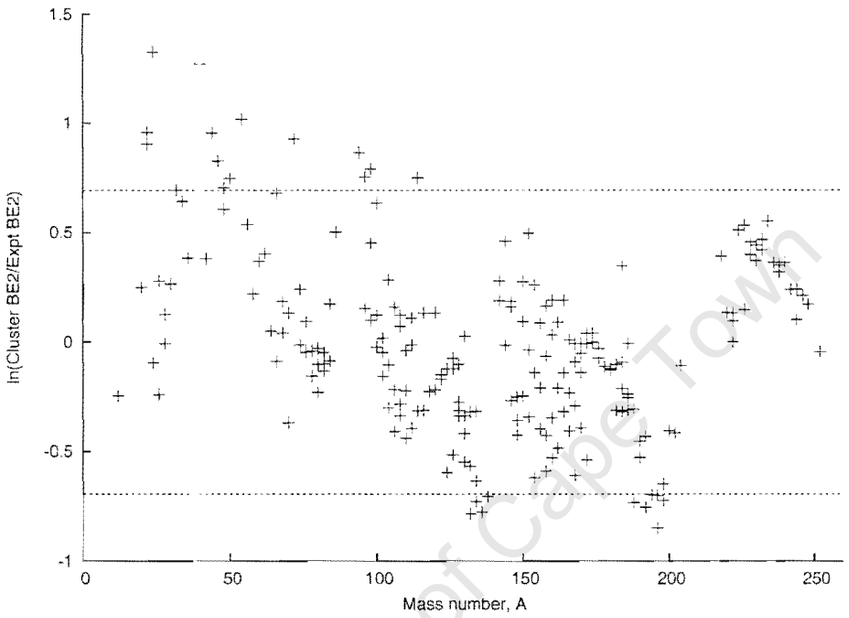

Figure 3.1: *Natural logarithm of ratio of calculated B(E2) (with $b = 0.35$) to experimental B(E2) against mass number A for non-magic nuclei. Factor 2 deviations are indicated by dashed lines.*

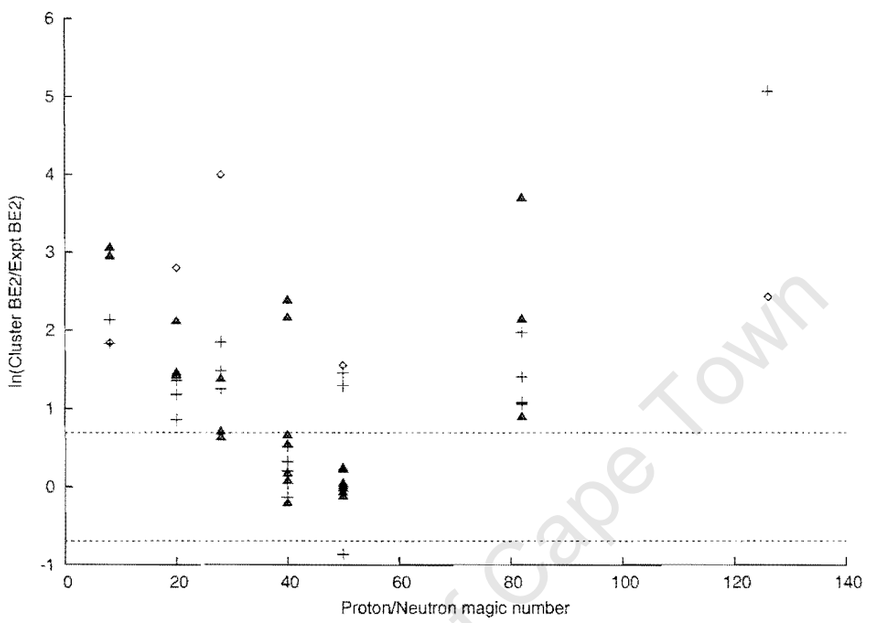

Figure 3.2: *Natural logarithm of ratio of calculated B(E2) (with $b = 0.35$) to experimental B(E2) against proton/neutron number Z/N. Triangles indicate magic proton numbers, crosses indicate magic neutron numbers, and open diamonds indicate doubly magic nuclei plotted by neutron number. Factor 2 deviations are indicated by dashed lines.*

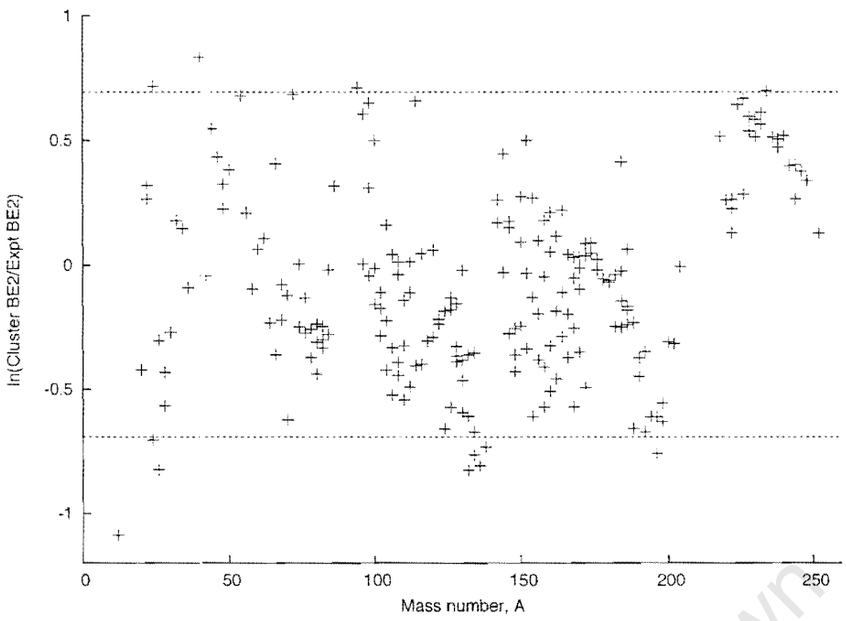

Figure 3.3: *Natural logarithm of ratio of calculated B(E2) (with* $b = 0.066A^{1/3}$*) to experimental B(E2) plotted against mass number A for non-magic nuclei. Factor 2 deviations are indicated by dashed lines.*

however, the results are in poor agreement with experiment, and we can see that the cluster model differentiates strongly between magic and non-magic nuclei. This differentiation is not as clear in the Bohr and Mottelson VRM models.

In a similar manner to earlier treatments [21, 23], a fit of the model to experiment has also been performed with a mass dependent normalization constant. A normalization constant of $b = 0.066A^{1/3}$ is used in Eq.(3.4) and the results of Figure 3.3 show an improvement over those of Figure 3.1.

3.3 Cluster-Core Decompositions from B(E2) values

As mentioned earlier, a most important requirement in any application of the cluster model is a method to determine the split of a nucleus into its cluster and core components. A number of these methods have been discussed in

Chapter 2 and have, in general, led to good agreement with the experimental data. Most of these methods have, however, been restricted to some part of the Periodic Table. For example, methods based on the observation of exotic decay can only be implemented for the Actinide region of the Periodic Table where exotic decay is observed. Even the maximum stability criterion often fails to supply well defined mass values for clusters and cores of nuclei throughout the Periodic Table.

We now derive a form for the reduced mass of a cluster-core system as a function of the charge, mass and B(E2) value of the parent nucleus [12]. Using the expression for the quadrupole transition strength derived from the cluster model (Eq.(2.14)) and setting $\psi_2 \sim \psi_0$, we have

$$B(E2) = \frac{1}{4\pi}\left[\frac{Z_1 Z_2}{Z}\int_0^\infty r^2 \psi_0^2 dr\right]^2 \tag{3.5}$$

Now, remembering that the expression for the no-dipole condition is:

$$\frac{Z_1}{A_1} = \frac{Z_2}{A_2} = \frac{Z}{A}$$

we then obtain for the reduced mass of the cluster-core system

$$\mu = \frac{A_1 A_2}{A} = \frac{Z_1 Z_2}{Z}\frac{A}{Z}$$

We can thus replace $\frac{Z_1 Z_2}{Z}$ in Eq.(3.5) with $\mu\frac{Z}{A}$. Replacing also the integral with $< r^2 >= r_0^2 A^{2/3}$, and r_0 some constant to be determined, leads to:

$$\mu = \frac{\sqrt{4\pi B(E2)}}{r_0^2}\frac{A^{1/3}}{Z} \tag{3.6}$$

This relation can be used to calculate μ, and hence the cluster-core decomposition, using only the mass, charge and experimentally determined B(E2) value of a given nucleus. As these values are known for many nuclei this relation may be far more widely applicable than previous methods of determining cluster-core decompositions. It can be used in conjunction with successful applications of the maximum stability criterion to determine the values of r_0. These values can then be averaged and used to determine μ in cases where the B(E2) is known, but the stability criterion gives inconclusive cluster-core decomposition values.

For example, the maximum stability criterion has supplied good results for cluster-core decompositions for ground state bands of nuclei adjacent to

closed shells, such as Ra, Th and U isotopes in the actinide region [10]. These particular isotopes yield seventeen cases [10] with μ ranging from 7.64 to 27.2, and result in values for r_0 in the range $r_0 = 1.21 \pm 0.04$ fm [12].

Good results have also been achieved using the stability criterion near closed shells in the rare-earth region. Here, the cluster model was applied to twelve cases of the isotopes Ba, Ce and Nd [25, 26], resulting in values of μ ranging from 6.62 to 17.2, generating an average value of $r_0 = 1.27 \pm 0.07$ fm [12].

We use this new expression for the reduced mass to generate the core and cluster masses and charges in the next chapter.

Chapter 4

Cluster Model Calculations of Yb Spectra

4.1 Overview

In this chapter we perform a full-scale implementation of the cluster model for a representative subset of even-even Yb isotopes. We use the expression for reduced mass, as derived in Section 3.3, to determine the reduced mass and hence the cluster-core configurations for these isotopes directly from their B(E2) values. We then generate cluster model nuclear spectra of these isotopes and compare them to corresponding experimental spectra [27].

Past implementations of the maximum stability criterion outlined in Section 2.1 encounter difficulties in identifying the cluster-core decompositions of the Yb isotopes: ^{158}Yb, ^{162}Yb, ^{166}Yb, ^{170}Yb and ^{174}Yb.

These difficulties are illustrated in Fig. 4.1, [A. C. Merchant, private communication], where the arrows correspond to cluster choices suggested by an application of Eq.(3.6) and which, as we shall see below, results in good fits to the Yb spectra. Although for the lighter isotopes a prominent local maximum in the D-plots exists near the required value of Z_2, for the heavier isotopes this is clearly not the case (indeed, smoothing the D-plots results in a local minimum at the required value).

We thus proceed to test our new method of cluster-core decomposition, based on the experimental B(E2) value.

To find the cluster and core masses and charges of the Yb isotopes, we begin

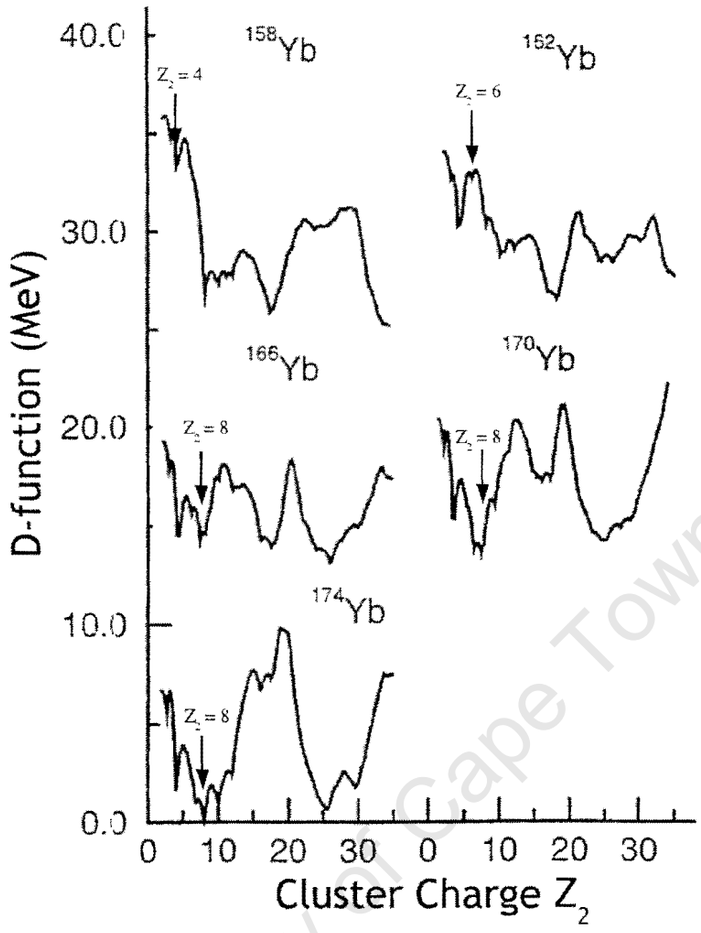

Figure 4.1: *D-plots for some Yb isotopes*

by applying the relation from Eq.(3.6)

$$\mu = \frac{A_1 A_2}{A} = \frac{\sqrt{4\pi B(E2)}}{r_0^2}\frac{A^{1/3}}{Z}$$

This, together with the condition $A = A_1 + A_2$, allows us to extract A_1 and A_2 for any nucleus for which the B(E2) is known, given a value for r_0. A good overall description of the Yb spectra is obtained using $r_0 = 1.35$ fm, consistent with the range of values obtained for other nuclei in the rare-

Earth region (see Section 3.3 and [12]). Next, using the no-dipole condition from Eq.(2.12)

$$\frac{Z_1}{A_1} = \frac{Z_2}{A_2} = \frac{Z}{A}$$

we can generate the cluster and core charges Z_2 and Z_1 as well. In general, the above treatment results in non-integer masses and charges (corresponding to a mixture of cluster-core configurations for each nuclei). We select the nearest even values for mass and charge of the components and these values are shown in Table 4.1.

Table 4.1. Cluster and core masses and charges for even-even Yb isotopes.

Isotope	B(E2)(e^2fm^4)	μ	Q(MeV)	A_1	A_2	Z_1	Z_2
^{158}Yb	3180	8.471	8.358	150	8	66	4
^{162}Yb	7000	12.673	13.460	148	14	64	6
^{166}Yb	10280	15.484	18.537	148	18	62	8
^{170}Yb	11420	16.450	14.782	152	18	62	8
^{174}Yb	11880	16.908	13.200	156	18	62	8

A note should be made here regarding the cluster-core decomposition of ^{158}Yb. The B(E2) value given in [23] is, in fact, 3700 $\pm$ 520 e^2fm^4 which results in the cluster-core decomposition:

$$^{158}_{70}\text{Yb} \rightarrow ^{148}_{66}\text{Dy} + ^{10}_{4}\text{Be}$$

and a poor fit to the ^{158}Yb spectrum. The error on the ^{158}Yb B(E2) value is however relatively large compared to the rest of the Yb isotopes. Using the lower limit B(E2) = 3180 e^2fm^4 results in the cluster-core decomposition shown in Table 4.1, i.e.

$$^{158}_{70}\text{Yb} \rightarrow ^{150}_{66}\text{Dy} + ^{8}_{4}\text{Be}$$

and an improved fit to the ^{158}Yb spectrum.

In order to generate spectra using the cluster model, an appropriate potential $V_T(r)$ acting between the cluster and core must be chosen. As described in Section 2.2 this potential consists of a nuclear term $V_N(r)$, a Coulomb interaction term $V_C(r)$, and a term representing the Langer form of the centrifugal potential, and is given by

$$V_T(r) = V_N(r) + V_C(r) + \frac{\hbar^2(L+0.5)^2}{2\mu r^2} \tag{4.1}$$

For the current implementation the mass symmetric form of the modified Woods-Saxon potential is used for the nuclear term $V_N(r)$ (see Eq.(2.4)). The Coulomb term $V_C(r)$ is taken to be the Coulomb interaction between a charged sphere, representing the core, and a point charge, representing the nuclear cluster. (See Eqs.(2.5) and (2.6)). We set the Coulomb potential radius, R_C, equal to the nuclear potential radius, R, to reduce the number of parameters.

As in earlier work [18] the parameters of this general potential are fixed at $V_0 = 54$ MeV, $x = 0.33$, and $a = 0.73$ fm for all nuclei, except for the nuclear radius, R, which is fitted to each individual nucleus. In all the earlier work of Buck et al R was chosen so as to reproduce the energy of a single level of a band (usually the 0^+ bandhead). A novel feature of the present analysis is that the value of R is chosen to optimise the overall fit to the energies E_L in the ground state band. Thus, for a given cluster and core, our choice of R minimises the value of the function S given by

$$S = \sum_L [E_L(\text{Expt}) - E_L(\text{Theor})]^2 \tag{4.2}$$

where $L^\pi = 0^+, 2^+, \ldots 20^+$. It should be noted that for ^{158}Yb we fit only even parity states up to the 12^+ state, as states beyond this are indicative (by the sudden change of level spacing above the 12^+ state) of not belonging to the ground state band. For ^{166}Yb, ^{170}Yb and ^{174}Yb the states above 16^+, 12^+ and 10^+ respectively are also less certain, but for uniformity we fit the spectra up to the 20^+ state. It is interesting also to note that, excepting for the case of ^{162}Yb where an inferior fit to the spectrum is obtained, the values of R group very closely together.

We use the Bohr-Sommerfeld relation from Eq.(2.8) along with the cluster-core potential described above to generate spectra. The value of the global quantum number, G, required by the Bohr-Sommerfeld relation is determined from the relation $G = gA_2$ [5] where A_2 is the cluster mass and $g = 4$ for Yb isotopes in the rare-Earth region of the Periodic Table.

4.2 Spectra

Figures 4.2 - 4.6 below show the cluster model generated spectra compared with the experimental spectra. Table 4.2 shows the fitted R values with the corresponding least squared values for the fits.

TABLE 4.2. Fitted R-values for the Yb isotopes and corresponding values of sum of squared deviations S.

Isotope	R (fm)	S
^{158}Yb	5.74192	0.083
^{162}Yb	5.64426	0.521
^{166}Yb	5.75401	0.132
^{170}Yb	5.77381	0.022
^{174}Yb	5.77263	0.037

In general, good agreement of the cluster model generated spectra with experimental spectra is obtained, with consistent values of R. In particular the experimental compression of the spectra as the mass (and deformation) increases from ^{158}Yb to ^{174}Yb is well reproduced. This can be traced to the corresponding increase in cluster mass. ^{162}Yb presents a slightly anomalous case, however, with the fit to the experimental spectrum being less good than those of its neighbouring isotopes and yielding a fitted R value significantly different from the rest of the Yb isotopes.

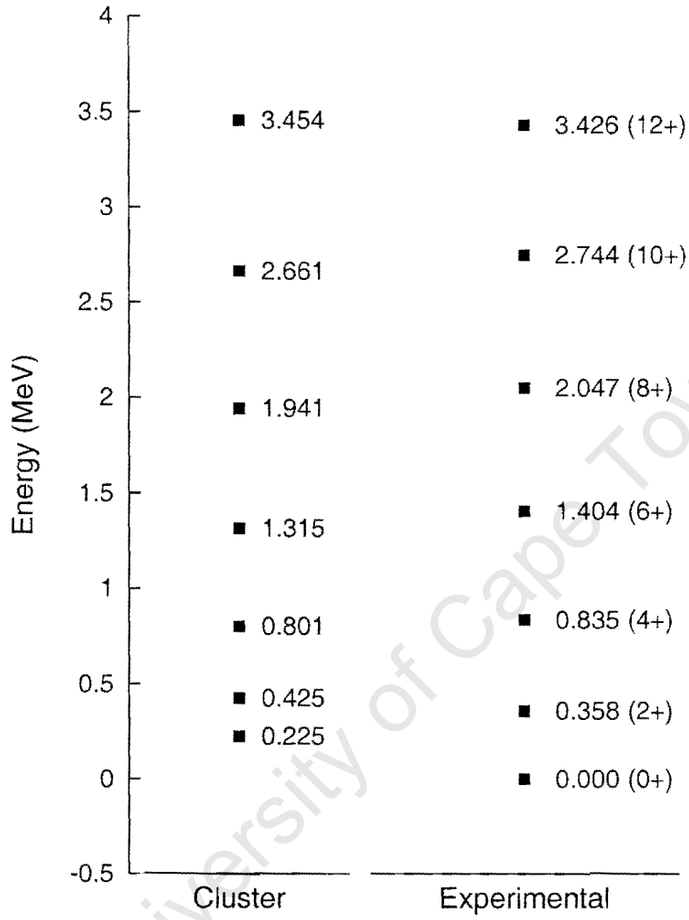

Figure 4.2: *Comparison of theoretical and experimental spectra for* ^{158}Yb.

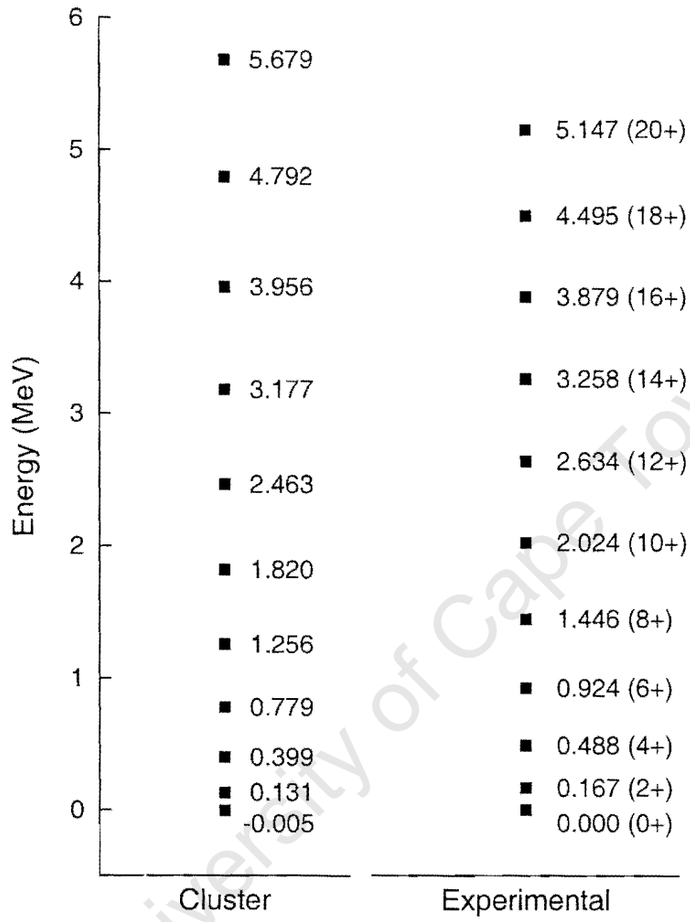

Figure 4.3: *Comparison of theoretical and experimental spectra for* ^{162}Yb

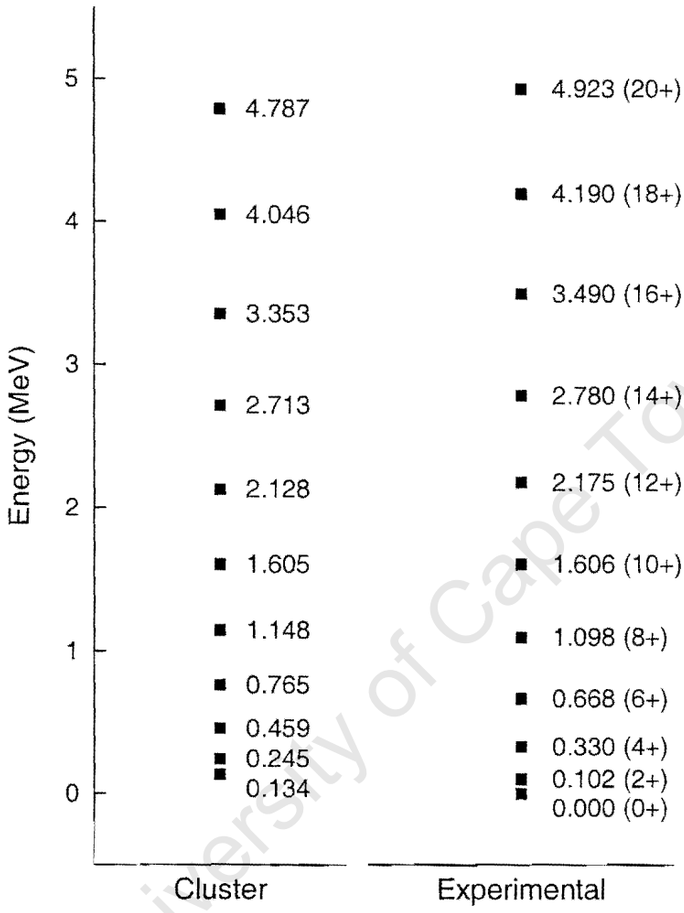

Figure 4.4: *Comparison of theoretical and experimental spectra for* ^{166}Yb.

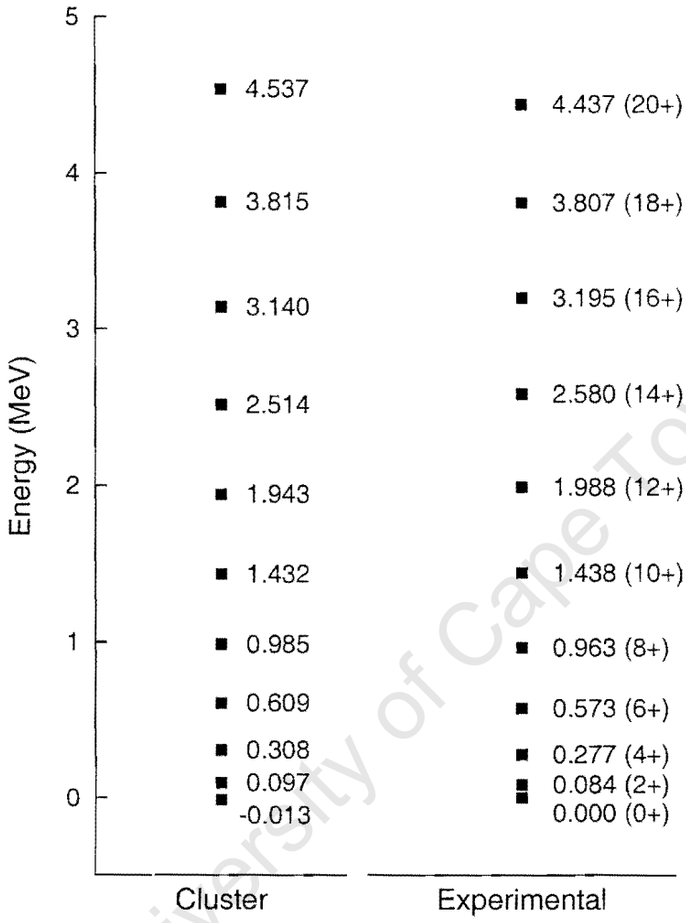

Figure 4.5: *Comparison of theoretical and experimental spectra for* ^{170}Yb.

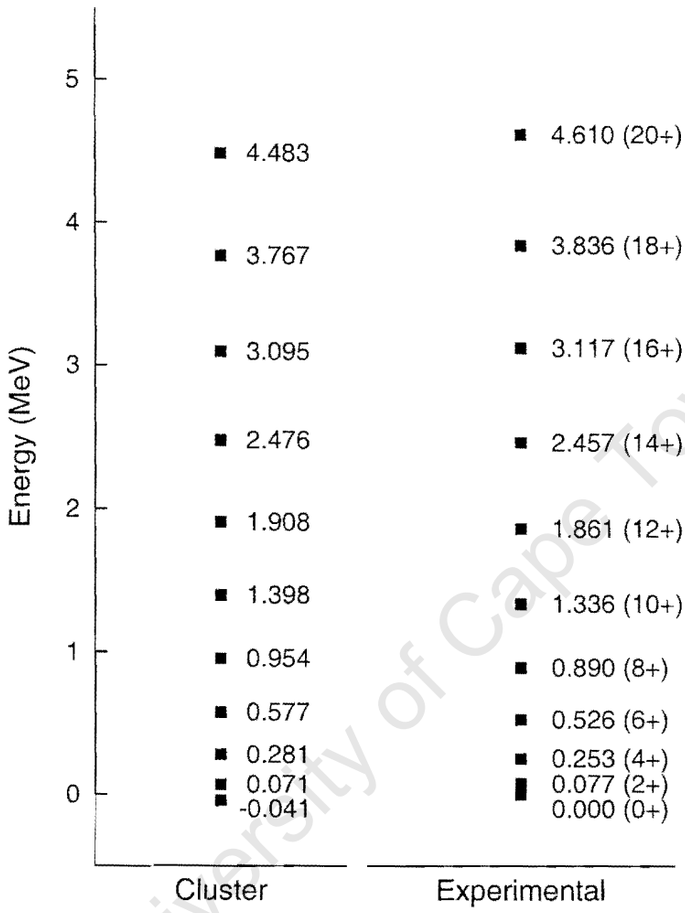

Figure 4.6: *Comparison of theoretical and experimental spectra for* ^{174}Yb.

Chapter 5

Cluster-Core Decompositions from Energy Levels

In Chapter 4, cluster-core decompositions of the Yb isotopes were determined by the method described in Section 3.3, whereby the experimental B(E2) value gives rise to the reduced mass of the cluster-core system, which in turn gives rise to the cluster and core masses. The cluster and core charges are then determined from the no-dipole condition. It may then be worthwhile to consider the following approach: since the excitation energies and B(E2) values are linked (by Eq.(3.3)), and we are able to determine the cluster-core system from the experimental B(E2) values, we may be able to derive cluster-core decompositions from the experimental spectra alone.

This chapter focuses on implementing the above idea by selecting a few possible clusters and corresponding cores for a given nucleus, and then using a least squares fitting algorithm to fit the cluster generated energy levels to the corresponding experimental levels. The best cluster-core combination for the given nucleus is the one which results in an overall minimum for the value of S as defined by Eq.(4.2).

5.1 Implementation

As the calculations are quite time-consuming (see Appendix B), in these preliminary calculations we apply the technique to just two typical cases, ^{162}Yb and ^{170}Yb. For each of these isotopes we could in principle run through all possible cluster-core decompositions, but here we confine ourselves to a likely

set suggested by our previous calculations. Thus for ^{162}Yb we choose the cluster charges $Z_2 = 4, 6$ and 8, and for each charge select cluster masses bracketing the Z/A values of ^{162}Yb so as to approximately satisfy the no-dipole criterion. For ^{162}Yb we thus use the clusters ^{8}Be, ^{10}Be, ^{12}Be, ^{12}C, ^{14}C, ^{16}C, ^{16}O, ^{18}O and ^{20}O. Similarly for ^{170}Yb we select $Z_2 = 6, 8$ and 10 and the clusters ^{14}C, ^{14}C, ^{16}C, ^{16}O, ^{18}O, ^{20}O, ^{20}Ne, ^{22}Ne and ^{24}Ne.

In order to generate the energy spectra for a given nucleus using the cluster model we require:

- the cluster-core decomposition
- the interaction between core and cluster
- the quantum numbers of the cluster-core relative motion

The cluster-core decompositions of interest are discussed in the paragraph above. For the interaction between the cluster and core we use the potential $V_T(r)$ of Eq.(4.1), comprising nuclear, Coulomb and centrifugal terms as specified in the discussion following that equation. For the global quantum number G we again use $G = 4A_2$ where A_2 is the cluster mass.

For each cluster-core decomposition we then keep all potential parameters fixed, except for the nuclear potential radius R_0 which is varied in order to optimize the fit between the experimental energies and the theoretical energies obtained using the Bohr-Sommerfeld relation. The optimal cluster-core decomposition is then the one which results in the best of these fits. Ideally, we'd like the cluster-core configuration which comes out of this method to be the same as that obtained using Eq.(3.6) for the reduced mass. This would provide further evidence for clustering in nuclei, as the cluster-core configurations are derived from different criteria.

5.2 Examples

We have implemented this approach for the two isotopes: ^{162}Yb and ^{170}Yb. These were chosen as we have already calculated cluster-core decompositions for them in Chapter 4 and thus they allow a comparison of our two methods of generating these decompositions.

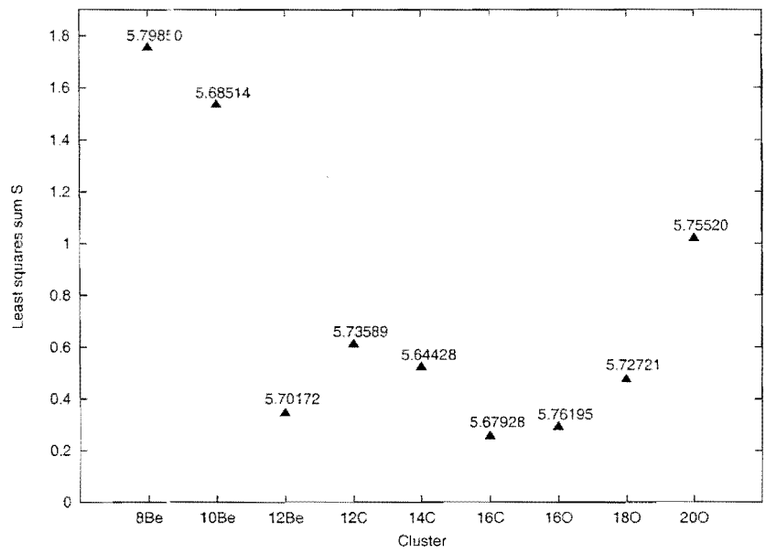

Figure 5.1: *The least squares sum S plotted for a range of clusters of* ^{162}Yb. *The values above the points represent the fitted values of R, the nuclear radius.*

In Figures 5.1 and 5.2, the value of S defined as in Eq.(4.2) by

$$S = \sum_{L} [E_L(\text{Expt}) - E_L(\text{Theor})]^2$$

with $L = 0^+, 2^+ \ldots 20^+$ is shown for the best fit obtained by varying the nuclear potential radius R for each cluster. Values of the fitted R are shown alongside the points.

For ^{162}Yb, there is a double minimum for the clusters ^{12}Be and ^{16}C/^{16}O, with fitted R-values of 5.70172 fm and 5.67928/5.76195 fm respectively. Looking back to Chapter 4, the implementation of the reduced mass method (Eq.(3.6)) for determining cluster-core decompositions yields the cluster ^{14}C, but with a significantly worse than average fit to the experimental energy level spectrum. It is clear that an ambiguity in the choice of cluster-core decomposition for ^{162}Yb exists. This can be resolved by fitting only states up to the 12^+ state [S. M. Perez, private communication]. This approach yields a single, well-defined minimum at the cluster ^{12}C with a fitted R-value of 5.73459 fm - much closer to the fitted R-values of the rest of the

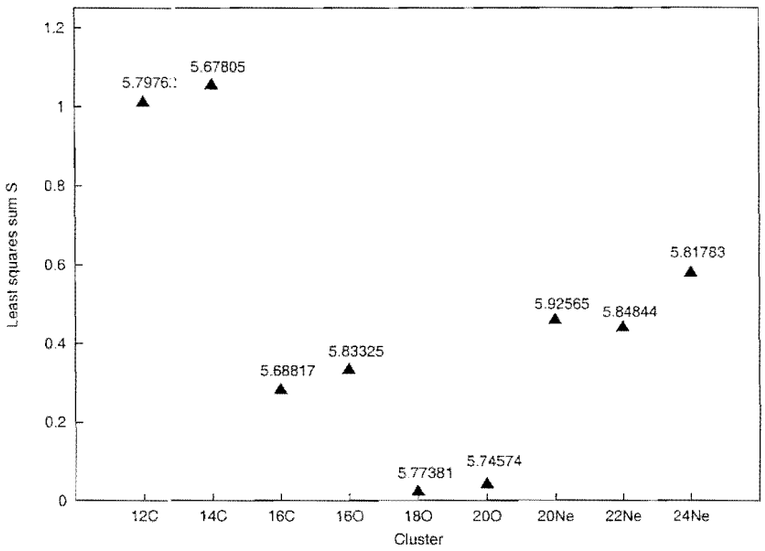

Figure 5.2: *The least squares sum S plotted for a range of clusters of* ^{170}*Yb. The values above the points represent the fitted values of R, the nuclear radius.*

Yb isotopes. These two factors could well indicate that levels above the 12^+ state may be described by a different cluster-core decomposition from those levels below 12^+.

The results for ^{170}Yb are quite different in appearance. Here there is a well-defined minimum at cluster values ^{18}O and ^{20}O. ^{18}O corresponds to the cluster determined from the reduced mass in Chapter 4 (see Table 4.1), and thus the fit to experimental energy levels yields a result consistent with that obtained by using the method described in Chapter 3.

Although the above results are promising it is clear that further tests of and refinements to this method are required before it can be applied confidently to any given nucleus. The least squares value gives an indication of the *overall* best fit to the experimental spectrum. In all of the fitted spectra (see Figures 4.2 - 4.6) it is found that the higher L^π states have a better relative fit to experimental levels than the lower energy L^π states. Thus, fitting to, say, the first five L^π states may yield a different result than when fitting to the first ten L^π states. It may be possible for future methods to

employ a weighting technique that would eliminate this effect and further investigation is clearly necessary.

Chapter 6

Summary and Conclusion

The dissertation begins with an introduction to various widely used models of nuclear structure, the shell, collective, and cluster models. Following this the fundamental ingredients of a cluster model are discussed in detail, i.e. the choices of an appropriate cluster-core decomposition, of the cluster-core interaction, and of the quantum numbers of the cluster-core relative motion. Various cluster model based derivations and calculations are then undertaken, summarised by the following four points:

1. A new relation between the quadrupole transition strengths and excitation energies of nuclei is derived in a cluster model context. B(E2) values calculated from this relation (in the mass region $A = 12$ to 252) show good agreement with both experimental values and B(E2) values generated by the vibrational and rotational (VRM) models of Bohr and Mottelson. Cluster model B(E2) values of magic nuclei do, however, show significantly greater deviation from experimental B(E2) values of magic nuclei than do the B(E2) values generated by the VRM models. In this context the cluster model differentiates strongly between magic and non-magic nuclei.

2. Following from the relation described in point 1, an expression for the reduced mass of the cluster-core system, dependent on A, Z and the experimental B(E2) value, is derived. This allows the extraction of cluster-core decompositions for any nucleus for which an experimental B(E2) value is available.

3. Tests of the above method of determining likely cluster-core decom-

positions are undertaken. A representative set of even-even Yb isotopes, for which a previous maximum stability method of choosing cluster-core decompositions yields poor results, is chosen for these tests. Theoretical spectra generated using cluster-core decompositions obtained from experimental B(E2) values show good agreement with experimental spectra for these isotopes. The only free parameter in the calculations, the nuclear potential radius R, shows no unphysical strong variation from isotope to isotope, remaining practically constant throughout.

4. A further method for determining likely cluster-core decompositions by least squares fits to nuclear energy level spectra is investigated. Using two Yb isotopes from the original dataset, theoretical cluster model spectra are fitted to experimental spectra for a range of cluster-core decompositions for each nucleus, with the resulting best fitted spectrum indicating the favoured cluster-core decomposition. Results for the two nuclei are promising, but a larger dataset and further refinement of the fitting procedure are required in future studies.

In conclusion a number of successful applications of the cluster model has resulted from the work, as well as some indications of where further development may prove useful.

Bibliography

[1] C. J. Batty, G. W. Greenlees, Nucl. Phys. **A133**, 673 (1969)

[2] P. E. Hodgson, *The optical model of elastic scattering* (Claredon Press, Oxford, 1963)

[3] W. E. Burcham, Elements of Nuclear Physics (Longman, New York, 1981)

[4] B. Buck, A. C. Merchant, and S. M. Perez, Phys. Rev. C **53** 2841 (1996)

[5] B. Buck, A. C. Merchant and S. M. Perez, Phys. Rev. Lett.**76**, 380 (1996)

[6] B. Buck, A. C. Merchant and S. M. Perez, Phys. Rev. C **58**, 2049 (1998)

[7] M. Freer and A. C. Merchant, J. Phys. **G23**, 261 (1997)

[8] P. E. Hodgson and E. Betak, Physics Reports 374, 1 (2003)

[9] B. Buck, A. C. Merchant and S. M. Perez, Phys. Rev. C**51**, 559 (1995)

[10] B. Buck, A. C. Merchant, M. J. Horner and S. M. Perez, Phys. Rev. C **61**, 024314 (2000)

[11] W. S. C. Williams, *Nuclear and Particle Physics* (Clarendon Press, Oxford, 1991)

[12] B. Buck, A. C. Merchant, V. A. McBride and S. M. Perez, Phys. Rev. C **66**, 067303 (2002)

[13] C. J. Batty, E. Friedman, H. J. Gils and H. Rebel, Adv. Nucl. Phys. **19** 1 (1989)

[14] F. Michel, J. Albinski, P. Belery, Th. Delbar, Gh. Gregoire, B. Tasiaux, and G. Reidermeister, Phys. Rev. C **28**, 1904 (1983)

[15] F. Michel, G. Reidermeister, S. Ohkubo,Phys. Rev. C **37**, 292, 1998

[16] B. Buck, J. C. Johnston, A. C. Merchant and S. M. Perez, Phys. Rev. C **52** 1840 (1995)

[17] B. Buck, J. C. Johnston, A. C. Merchant and S. M. Perez, Phys. Rev. C **53** 2841 (1996)

[18] B. Buck, A. C. Merchant and S. M. Perez, Nucl. Phys **A614** 129 (1997)

[19] B. Buck, H. Friedrich, G. Wheatley, Nucl. Phys. **A275**, 246 (1977)

[20] B. Buck, P. J. B. Hopkins, and A. C. Merchant, Nucl. Phys. **A513**, 75 (1990)

[21] L. Grodzins, Phys. Lett. **2**, 88 (1962)

[22] A. Bohr and B. R. Mottelson, Mat. Fys. Medd. K. Dan. Vidensk. Selsk.**27** 16 (1953)

[23] S. Raman, C. W. Nestor, S. Kahane, and K. H. Bhatt, At. Data Nucl.Data Tables **42**, 1 (1989)

[24] B. Buck, A. C. Merchant and S. M. Perez, Phys. Rev. C **59**, 750 (1999)

[25] B. Buck, A. C. Merchant and S. M. Perez, Nucl. Phys **A652** 211 (1999)

[26] B. Buck, A. C. Merchant and S. M. Perez, Nucl. Phys **A657** 267 (1999)

[27] V. A. McBride and S. M. Perez, SAIP 48th Annual Conference, Stellenbosch, South Africa, June 2003, Abstract **B36**

Appendix A

Data and Comparison of VRM and Cluster Results

A.1 Non-magic data

Energies in MeV and B(E2) = B(E2: $2^+ \rightarrow 0^+$) values in $e^2\mathrm{fm}^4$. Energies from appropriate Nucl. Data Sheets. Expt B(E2) and VRM B(E2) values deduced from the B(E2: $0^+ \rightarrow 2^+$) values in $e^2\mathrm{b}^2$ of Raman et al [23]. Cluster B(E2) values from Eq.(3.4) with $b = 0.35$, $L = 4$ and $l = 2$.

A	Z	E_2^*	E_4^*	Expt B(E2)			VRM B(E2)	Cluster B(E2)
12	6	4.4389	14.0830	8.2	±	1.0	5	6.409E+00
20	10	1.6337	4.2477	68.0	±	6.0	32	8.724E+01
22	10	1.2745	3.3572	46.0	±	2.0	38	1.136E+02
24	10	1.9808	3.9620	28.0	±	12.0	24	1.055E+02
22	12	1.2460	3.3082	64.0	±	24.0	56	1.668E+02
24	12	1.3686	4.1229	86.4	±	2.4	50	7.858E+01
26	12	1.8087	4.3184	61.0	±	2.6	36	8.065E+01
28	12	1.4725	4.0202	68.0	±	10.0	44	6.748E+01
26	14	1.7959	5.3300	70.4	±	6.8	50	5.536E+01
28	14	1.7789	4.6179	65.2	±	2.4	50	7.397E+01
30	14	2.2355	5.2800	43.0	±	2.0	38	5.603E+01
32	16	2.2302	4.4589	60.0	±	2.6	50	1.200E+02
34	16	2.1274	4.6890	42.4	±	2.4	52	8.048E+01
36	18	1.9704	4.4144	68.0	±	8.0	68	9.981E+01

A	Z	E_2^*	E_4^*	Expt B(E2)			VRM B(E2)	Cluster B(E2)
40	18	1.4608	2.8926	66.0	±	8.0	90	2.355E+02
42	18	1.2082	3.0962	84.0	±	20.0	106	1.229E+02
44	22	1.0832	2.4543	122.0	±	30.0	174	3.171E+02
46	22	0.8892	2.0098	190.0	±	10.0	208	4.343E+02
48	22	0.9834	2.2956	144.0	±	8.0	186	2.909E+02
48	24	0.7523	1.8586	266.0	±	40.0	280	4.871E+02
50	24	0.7833	1.8813	216.0	±	12.0	280	4.557E+02
54	24	0.8348	1.8239	174.0	±	8.0	240	4.815E+02
56	26	0.8468	2.0851	196.0	±	8.0	280	3.352E+02
58	26	0.8108	2.0765	240.0	±	8.0	300	2.991E+02
60	26	0.8236	2.1145	186.0	±	36.0	280	2.687E+02
62	30	0.9539	2.1861	246.0	±	18.0	320	3.677E+02
64	30	0.9915	2.3067	288.0	±	24.0	320	3.029E+02
66	30	1.0394	2.4510	270.0	±	20.0	300	2.472E+02
68	30	1.0774	2.4174	248.0	±	30.0	280	2.585E+02
66	32	0.9574	2.1738	192.0	±	36.0	360	3.789E+02
68	32	1.0161	2.2682	280.0	±	40.0	340	3.368E+02
70	32	1.0396	2.1534	352.0	±	8.0	320	4.017E+02
74	32	0.5959	1.4638	600.0	±	12.0	560	5.920E+02
76	32	0.5629	1.4101	536.0	±	16.0	600	5.890E+02
70	34	0.9454	2.0396	680.0	±	160.0	400	4.699E+02
72	34	0.8620	1.6369	350.0	±	40.0	440	8.856E+02
76	34	0.5591	1.3309	840.0	±	20.0	680	8.013E+02
78	34	0.6138	1.5026	670.0	±	18.0	600	5.735E+02
80	34	0.6664	1.7015	506.0	±	12.0	560	4.020E+02
82	34	0.6544	1.7351	368.0	±	10.0	560	3.510E+02
74	36	0.4557	1.0147	1420.0	±	300.0	940	1.806E+03
78	36	0.4553	1.1195	1200.0	±	100.0	920	1.151E+03
80	36	0.6162	1.4360	740.0	±	40.0	680	7.184E+02
82	36	0.7765	1.8205	466.0	±	20.0	520	4.216E+02
84	36	0.8815	2.0950	250.0	±	12.0	460	2.974E+02
80	38	0.3854	0.9808	1680.0	±	140.0	1200	1.518E+03
82	38	0.5734	1.3284	1026.0	±	40.0	800	8.983E+02

A	Z	E_2^*	E_4^*	Expt B(E2)			VRM B(E2)	Cluster B(E2)
84	38	0.7931	1.7679	560.0	±	80.0	580	5.135E+02
86	38	1.0766	2.2297	212.0	±	32.0	420	3.501E+02
98	38	0.1442	0.4338	1940.0	±	220.0	3000	4.276E+03
100	38	0.1292	0.4173	2200.0	±	100.0	3200	4.148E+03
94	42	0.8711	1.5737	406.0	±	8.0	620	9.643E+02
96	42	0.7783	1.6281	542.0	±	10.0	680	6.320E+02
98	42	0.7874	1.5100	534.0	±	10.0	660	8.388E+02
100	42	0.5356	1.1361	1032.0	±	20.0	980	1.166E+03
102	42	0.2966	0.7437	2120.0	±	240.0	1760	2.023E+03
104	42	0.1923	0.5606	2160.0	±	160.0	2600	2.867E+03
106	42	0.1717	0.5223	2600.0	±	140.0	3000	3.046E+03
108	42	0.1929	0.5368	2700.0	±	620.0	3000	3.049E+03
96	44	0.8326	1.5180	502.0	±	20.0	700	1.066E+03
98	44	0.6524	1.3978	784.0	±	24.0	880	8.651E+02
100	44	0.5396	1.2265	1002.0	±	20.0	1060	9.785E+02
102	44	0.4751	1.1064	1302.0	±	32.0	1200	1.113E+03
104	44	0.3580	0.8885	1682.0	±	32.0	1580	1.517E+03
108	44	0.2422	0.6652	2060.0	±	280.0	2300	2.212E+03
110	44	0.2407	0.6633	2220.0	±	260.0	2300	2.136E+03
112	44	0.2367	0.6449	2240.0	±	400.0	2340	2.209E+03
102	46	0.5564	1.2759	920.0	±	60.0	1120	9.368E+02
104	46	0.5558	1.3236	1070.0	±	70.0	1120	7.914E+02
106	46	0.5119	1.2293	1312.0	±	70.0	1200	8.725E+02
108	46	0.4340	1.0483	1520.0	±	80.0	1400	1.146E+03
110	46	0.3738	0.9208	1740.0	±	80.0	1620	1.394E+03
112	46	0.3488	0.8836	1260.0	±	200.0	1720	1.407E+03
114	46	0.3329	0.8523	680.0	±	200.0	1800	1.439E+03
116	46	0.3406	0.8776	1140.0	±	320.0	1760	1.300E+03
106	48	0.6327	1.4938	820.0	±	40.0	1060	6.595E+02
108	48	0.6329	1.5085	860.0	±	40.0	1040	6.144E+02
110	48	0.6578	1.5425	900.0	±	40.0	1000	5.801E+02

A	Z	E_2^*	E_4^*	Expt B(E2)			VRM B(E2)	Cluster B(E2)
112	48	0.6174	1.4156	1020.0	±	40.0	1060	6.875E+02
114	48	0.5583	1.2837	1100.0	±	40.0	1160	8.033E+02
116	48	0.5134	1.2194	1120.0	±	40.0	1260	8.190E+02
120	52	0.5604	1.1616	1540.0	±	320.0	1340	1.239E+03
122	52	0.5640	1.1814	1320.0	±	12.0	1320	1.137E+03
124	52	0.6027	1.2486	1136.0	±	12.0	1240	1.005E+03
126	52	0.6662	1.3613	950.0	±	20.0	1120	8.406E+02
128	52	0.7432	1.4973	766.0	±	12.0	1000	6.920E+02
130	52	0.8394	1.6330	590.0	±	14.0	880	6.058E+02
118	54	0.3373	0.8103	2800.0	±	140.0	2420	2.232E+03
120	54	0.3218	0.7959	1880.0	±	180.0	2600	2.148E+03
122	54	0.3313	0.8283	2240.0	±	200.0	2440	1.891E+03
124	54	0.3541	0.8790	2980.0	±	180.0	2260	1.641E+03
126	54	0.3885	0.9419	1540.0	±	50.0	2060	1.430E+03
128	54	0.4229	1.0331	1500.0	±	80.0	1800	1.140E+03
130	54	0.5361	1.2016	1300.0	±	100.0	1480	9.289E+02
132	54	0.6677	1.4403	920.0	±	60.0	1180	6.685E+02
134	54	0.8470	1.7312	680.0	±	120.0	920	4.954E+02
126	56	0.2558	0.7113	3800.0	±	420.0	3400	2.270E+03
128	56	0.2841	0.7634	2720.0	±	220.0	3000	1.987E+03
130	56	0.3573	0.9019	2580.0	±	280.0	2380	1.492E+03
132	56	0.4646	1.1277	1720.0	±	120.0	1820	9.761E+02
134	56	0.6047	1.4006	1360.0	±	320.0	1400	6.574E+02
136	56	0.8185	1.8666	800.0	±	100.0	1020	3.680E+02
142	56	0.3596	0.8348	1360.0	±	120.0	2300	1.642E+03
144	56	0.1993	0.5302	2080.0	±	120.0	4200	3.294E+03
146	56	0.1808	0.5135	2700.0	±	200.0	4600	3.169E+03
128	58	0.2073	0.6069	4300.0	±	360.0	4400	3.066E+03
130	58	0.2539	0.7104	3460.0	±	180.0	3600	2.278E+03
132	58	0.3254	0.8591	3540.0	±	280.0	2800	1.616E+03
134	58	0.4092	1.0489	2060.0	±	180.0	2200	1.092E+03

A	Z	E_2^*	E_4^*	Expt B(E2)			VRM B(E2)	Cluster B(E2)
142	58	0.6412	1.2194	900.0	±	20.0	1380	1.190E+03
146	58	0.2583	0.6683	1860.0	±	260.0	3400	2.239E+03
148	58	0.1585	0.5434	3780.0	±	300.0	5600	2.472E+03
150	58	0.0971	0.3061	6200.0	±	120.0	9000	8.162E+03
144	60	0.6965	1.3147	1100.0	±	60.0	1360	1.083E+03
146	60	0.4538	1.0422	1520.0	±	60.0	2080	1.163E+03
148	60	0.3017	0.7522	2760.0	±	60.0	3200	1.931E+03
150	60	0.1301	0.3815	5500.0	±	80.0	7200	6.040E+03
152	60	0.0725	0.2366	8400.0	±	1400.0	12800	1.380E+04
138	62	0.3469	0.8918	3280.0	±	700.0	3000	1.621E+03
148	62	0.5502	1.1615	1440.0	±	60.0	1820	1.120E+03
150	62	0.3339	0.7732	2700.0	±	60.0	3000	2.111E+03
152	62	0.1218	0.3664	6880.0	±	80.0	8200	6.631E+03
154	62	0.0820	0.2668	8720.0	±	100.0	12000	1.132E+04
152	64	0.3443	0.7554	3520.0	±	300.0	3000	2.501E+03
154	64	0.1231	0.3710	7700.0	±	100.0	8600	6.700E+03
156	64	0.0890	0.2882	9280.0	±	100.0	11800	1.011E+04
158	64	0.0795	0.2614	10040.0	±	100.0	13200	1.182E+04
160	64	0.0753	0.2485	10500.0	±	120.0	13800	1.271E+04
154	66	0.3345	0.7470	4780.0	±	240.0	3400	2.573E+03
156	66	0.1379	0.4042	7420.0	±	80.0	8000	6.016E+03
158	66	0.0989	0.3171	9320.0	±	100.0	11200	8.739E+03
160	66	0.0868	0.2838	10120.0	±	280.0	12800	1.045E+04
162	66	0.0807	0.2657	10560.0	±	300.0	13600	1.156E+04
164	66	0.0734	0.2422	11200.0	±	100.0	14800	1.355E+04
156	68	0.3444	0.7974	3280.0	±	140.0	3400	2.208E+03
158	68	0.1923	0.5272	6040.0	±	460.0	6200	3.938E+03
160	68	0.1256	0.3899	8720.0	±	360.0	9400	6.166E+03
162	68	0.1021	0.3296	10020.0	±	120.0	11400	8.116E+03
164	68	0.0914	0.2994	10900.0	±	120.0	12800	9.472E+03
166	68	0.0806	0.2650	11660.0	±	100.0	14400	1.177E+04

A	Z	E_2^*	E_4^*	Expt B(E2)			VRM B(E2)	Cluster B(E2)
168	68	0.0798	0.2641	11580.0	±	200.0	14400	1.150E+04
170	68	0.0786	0.2602	11640.0	±	200.0	14600	1.157E+04
158	70	0.3579	0.8352	3700.0	±	520.0	3400	2.054+E03
160	70	0.2431	0.6384	4960.0	±	440.0	5200	2.921E+03
162	70	0.1663	0.4876	7000.0	±	700.0	7400	4.314E+03
164	70	0.1233	0.3856	8680.0	±	480.0	10000	6.316E+03
166	70	0.1024	0.3305	10280.0	±	560.0	12000	8.148E+03
168	70	0.0877	0.2866	11460.0	±	200.0	14000	1.047E+04
170	70	0.0843	0.2775	11420.0	±	320.0	14400	1.083E+04
172	70	0.0788	0.2603	12080.0	±	140.0	15400	1.199E+04
174	70	0.0765	0.2531	11880.0	±	120.0	15800	1.237E+04
176	70	0.0821	0.2717	10820.0	±	200.0	14600	1.050E+04
166	72	0.1587	0.4706	6920.0	±	360.0	8200	4.611E+03
168	72	0.1237	0.3855	8560.0	±	440.0	10400	6.388E+03
170	72	0.1003	0.3220	10000.0	±	2200.0	12800	8.703E+03
172	72	0.0953	0.3092	8760.0	±	620.0	13400	9.126E+03
174	72	0.0910	0.2974	9600.0	±	580.0	14000	9.586E+03
176	72	0.0884	0.2902	10540.0	±	200.0	14400	9.797E+03
178	72	0.0932	0.3060	9640.0	±	120.0	13600	8.613E+03
180	72	0.0933	0.3086	9300.0	±	160.0	13600	8.232E+03
168	74	0.1993	0.5627	6440.0	±	320.0	6800	3.503E+03
170	74	0.1560	0.4625	7120.0	±	160.0	8800	4.810E+03
172	74	0.1229	0.3771	11700.0	±	960.0	11000	6.831E+03
180	74	0.1036	0.3375	8380.0	±	460.0	12800	7.364E+03
182	74	0.1001	0.3294	8300.0	±	220.0	13200	7.496E+03
184	74	0.1112	0.3641	7460.0	±	140.0	12000	6.033E+03
186	74	0.1226	0.3963	6880.0	±	120.0	10800	5.038E+03
182	76	0.1269	0.4000	7620.0	±	660.0	11000	5.574E+03
184	76	0.1198	0.3838	6400.0	±	300.0	11600	5.838E+03
186	76	0.1372	0.4341	5820.0	±	200.0	10200	4.516E+03
188	76	0.1550	0.4779	5080.0	±	120.0	9000	3.737E+03

A	Z	E_2^*	E_4^*	Expt B(E2)			VRM B(E2)	Cluster B(E2)
190	76	0.1867	0.5479	4600.0	±	180.0	7400	2.925E+03
192	76	0.2058	0.5803	4100.0	±	140.0	6600	2.664E+03
184	78	0.1630	0.4360	7900.0	±	280.0	9000	5.750E+03
186	78	0.1915	0.4903	5960.0	±	220.0	7600	4.698E+03
188	78	0.2656	0.6710	5200.0	±	940.0	5600	2.498E+03
190	78	0.2958	0.7370	3500.0	±	440.0	5000	2.064E+03
192	78	0.3165	0.7846	3820.0	±	120.0	4600	1.796E+03
194	78	0.3285	0.8113	3320.0	±	120.0	4400	1.653E+03
196	78	0.3557	0.8769	2800.0	±	80.0	4000	1.390E+03
198	78	0.4072	0.9851	2120.0	±	100.0	3600	1.108E+03
184	80	0.3667	0.6533	3880.0	±	900.0	4200	5.488E+03
186	80	0.4053	0.8080	2740.0	±	460.0	3800	2.720E+03
196	80	0.4261	1.0614	2300.0	±	100.0	3600	9.842E+02
198	80	0.4118	1.0485	1980.0	±	24.0	3600	9.603E+02
200	80	0.3680	0.9472	1706.0	±	22.0	4000	1.137E+03
202	80	0.4394	1.1199	1224.0	±	20.0	3400	8.078E+02
204	80	0.4366	1.1284	854.0	±	14.0	3400	7.664E+02
220	86	0.2410	0.5337	3720.0	±	140.0	7000	4.253E+03
222	86	0.1860	0.4484	4720.0	±	300.0	9000	5.198E+03
218	88	0.3892	0.7413	2120.0	±	380.0	4600	3.134E+03
222	88	0.1109	0.3014	9040.0	±	760.0	15800	1.033E+04
224	88	0.0844	0.2508	7980.0	±	320.0	20800	1.329E+04
226	88	0.0676	0.2115	10260.0	±	560.0	26000	1.745E+04
228	88	0.0638	0.2047	12020.0	±	980.0	28000	1.790E+04
222	90	0.1833	0.4398	5960.0	±	500.0	10000	5.957E+03
226	90	0.0721	0.2264	13700.0	±	800.0	26000	1.588E+04
228	90	0.0578	0.1868	14140.0	±	540.0	32000	2.231E+04
230	90	0.0532	0.1741	16080.0	±	200.0	34000	2.499E+04
232	90	0.0494	0.1621	18560.0	±	180.0	36000	2.823E+04
234	90	0.0496	0.1630	15800.0	±	1400.0	36000	2.741E+04
230	92	0.0518	0.1695	19000.0	±	2200.0	36000	2.754E+04

A	Z	E_2^*	E_4^*	Expt B(E2)			VRM B(E2)	Cluster B(E2)
232	92	0.0476	0.1566	19800.0	$\pm$	1600.0	40000	3.158E+04
234	92	0.0435	0.1433	21320.0	$\pm$	400.0	44000	3.697E+04
236	92	0.0452	0.1495	23220.0	$\pm$	300.0	42000	3.335E+04
238	92	0.0449	0.1484	24180.0	$\pm$	400.0	42000	3.326E+04
238	94	0.0441	0.1460	25220.0	$\pm$	340.0	44000	3.584E+04
240	94	0.0428	0.1417	26040.0	$\pm$	600.0	46000	3.742E+04
242	94	0.0445	0.1473	26800.0	$\pm$	320.0	44000	3.407E+04
244	94	0.0450	0.1530	27360.0	$\pm$	320.0	44000	3.034E+04
244	96	0.0429	0.1423	29340.0	$\pm$	340.0	48000	3.732E+04
246	96	0.0429	0.1420	29880.0	$\pm$	340.0	48000	3.693E+04
248	96	0.0434	0.1436	29980.0	$\pm$	360.0	46000	3.559E+04
252	98	0.0457	0.1519	33400.0	$\pm$	2200.0	46000	3.196E+04

A.2 Proton magic data

Energies in MeV and B(E2) = B(E2: $2^+ \rightarrow 0^+$) values in $e^2\mathrm{fm}^4$. Energies from appropriate Nucl. Data Sheets. Expt B(E2) and VRM B(E2) values deduced from the B(E2: $0^+ \rightarrow 2^+$) values in $e^2\mathrm{b}^2$ of Raman et al [23]. Cluster B(E2) values from Eq.(3.4) with $b = 0.35$, $L = 4$ and $l = 2$.

A	Z	E_2^*	E_4^*	Expt B(E2)			VRM B(E2)	Cluster B(E2)
16	8	6.9171	10.3560	8.0	±	0.8	5	5.041E+01
18	8	1.9822	3.5548	9.0	±	0.4	17	1.905E+02
20	8	1.6737	3.5700	5.6	±	0.4	19	1.061E+02
40	20	3.9043	5.2788	19.2	±	3.2	42	3.155E+02
42	20	1.5242	2.7524	84.0	±	6.0	104	3.584E+02
44	20	1.1570	2.2831	94.0	±	4.0	134	3.885E+02
46	20	1.3460	2.5747	36.2	±	2.6	114	2.986E+02
48	20	3.8317	4.5034	16.8	±	5.6	40	9.176E+02
58	28	1.4545	2.4591	139.0	±	0.8	192	5.506E+02
60	28	1.3325	2.5058	186.6	±	3.0	206	3.773E+02
62	28	1.1731	2.3364	178.0	±	5.0	232	3.594E+02
64	28	1.3459	2.6101	152.0	±	16.0	200	2.856E+02
84	40	0.5400	1.2630	874.0	±	48.0	920	1.034E+03
86	40	0.7519	1.6666	320.0	±	60.0	660	6.166E+02
88	40	1.0569	2.1396	520.0	±	180.0	460	4.203E+02
90	40	2.1862	3.0769	126.0	±	10.0	224	5.937E+02
92	40	0.9345	1.4955	166.0	±	12.0	520	1.432E+03
94	40	0.9182	1.4696	132.0	±	28.0	520	1.420E+03
100	40	0.2127	0.5645	1800.0	±	220.0	2220	3.083E+03
102	40	0.1518	0.4783	3200.0	±	640.0	3200	3.440E+03
112	50	1.2572	2.2476	480.0	±	28.0	560	4.845E+02
114	50	1.3000	2.1875	460.0	±	100.0	540	5.824E+02
116	50	1.2935	2.3909	418.0	±	12.0	540	3.679E+02
118	50	1.2296	2.2803	418.0	±	16.0	560	3.878E+02
120	50	1.1712	2.1945	404.0	±	8.0	600	3.954E+02
122	50	1.1406	2.1421	384.0	±	8.0	600	3.993E+02

A	Z	E_2	E_4^*	Expt B(E2)			VRM B(E2)	Cluster B(E2)
124	50	1.1316	2.1017	332.0	±	8.0	600	4.119E+02
204	82	0.8992	1.2739	324.0	±	8.0	1740	2.744E+03
206	82	0.8031	1.6840	200.0	±	4.0	1940	4.869E+02
208	82	4.0854	4.3232	580.0	±	60.0	380	6.554E+03
210	82	0.8000	1.0977	102.0	±	30.0	1940	4.102E+03

A.3 Neutron magic data

Energies in MeV and B(E2) = B(E2: $2^+ \rightarrow 0^+$) values in $e^2\text{fm}^4$. Energies from appropriate Nucl. Data Sheets. Expt B(E2) and VRM B(E2) values deduced from the B(E2: $0^+ \rightarrow 2^+$) values in $e^2\text{b}^2$ of Raman et al [23]. Cluster B(E2) values from Eq.(3.4) with $b = 0.35$, $L = 4$ and $l = 2$.

A	Z	N	E_2^*	E_4^*	Expt B(E2)			VRM B(E2)	Cluster B(E2)
14	6	8	7.0120	10.7360	3.7	±	0.5	3	3.158E+01
18	10	8	1.8873	3.3762	53.2	±	5.0	28	3.320E+02
36	16	20	3.2910	6.5144	19.2	±	5.2	32	4.533E+01
38	18	20	2.1676	4.4800	25.8	±	2.0	62	1.001E+02
42	22	20	1.5550	2.6766	160.0	±	46.0	124	5.201E+02
50	22	28	1.5537	2.6749	58.0	±	8.0	116	3.672E+02
52	24	28	1.4341	2.3696	132.0	±	6.0	148	5.803E+02
54	26	28	1.4077	2.5381	124.0	±	10.0	174	4.326E+02
70	30	40	0.8848	1.7865	320.0	±	28.0	340	5.387E+02
72	32	40	0.8340	1.7284	426.0	±	12.0	400	5.888E+02
74	34	40	0.6348	1.3632	774.0	±	16.0	600	9.487E+02
76	36	40	0.4238	1.0346	1640.0	±	80.0	1000	1.434E+03
86	36	50	1.5646	2.2502	244.0	±	20.0	260	8.890E+02
78	38	40	0.2785	0.7820	2140.0	±	260.0	1680	2.232E+03
88	38	50	1.8360	4.2272	184.0	±	10.0	244	7.776E+01
92	42	50	1.5093	2.2826	194.0	±	12.0	360	8.311E+02
136	54	82	1.3132	1.6944	360.0	±	160.0	600	2.587E+03
138	56	82	1.4359	1.8986	452.0	±	18.0	580	1.834E+03
140	58	82	1.5965	2.0832	592.0	±	12.0	560	1.728E+03
142	60	82	1.5758	2.1007	540.0	±	16.0	600	1.545E+03
144	62	82	1.6602	2.1909	532.0	±	16.0	600	1.570E+03
210	84	126	1.1814	1.4267	40.0	±	8.0	1380	6.341E+03

Appendix B

Description of Computer Code

This appendix describes the program used in this thesis to fit the cluster model generated energy levels E_L(Theor) to the experimental levels E_L(Expt). The program determines the value of the nuclear radius, R, which allows the closest match of the energy levels generated by the cluster model to the experimental levels.

The main program takes the following parameters as input:

A	the mass of the parent nucleus
A_2	the mass of the cluster
Z	the charge of the parent nucleus
Z_2	the charge of the cluster
R	the nuclear radius
dR	the step size of R
μ	the reduced mass of the cluster-core system
E_L	the entire band of experimental energy levels E_L(Expt) of the nucleus

For the input value of R, each individual energy level (E_L(Theor)) is calculated by calling a subroutine - *energy* - for the corresponding value of L. This subroutine begins with a guess E'_L at E_L(Theor) and implements the Bohr-Sommerfeld relation given in Chapter 2, Eq.(2.8). For convenience, this relation is given again below:

$$\int_{r_1}^{r_2} dr \sqrt{\frac{2\mu}{\hbar^2}\left[E'_L - V_T(r)\right]} = (G - L + 1)\frac{\pi}{2}$$

In order to perform the integral, the program must first determine the potential $V_T(r)$ and the classical turning points r_1 and r_2. The potential $V_T(r)$ consists of 3 terms, as mentioned in Chapter 2:

1. the nuclear potential $V_N(r)$, for which we use the mass-symmetric form given by Eq.(2.4)

2. the Coulomb potential $V_C(r)$ between a spherical, charged core and a point cluster, given by Eqs.(2.5) and (2.6)

3. the Langer modified centrifugal potential term

$$\frac{\hbar^2(L+0.5)^2}{2\mu r^2}$$

The total potential $V_T(r)$ is calculated in steps of 0.001 fm up to a distance of 15 fm from the origin by calling another subroutine - *ybpot* . The values for the potential at each discrete distance are calculated once for each L-value and then stored in an array.

The program then exits the *ybpot* subroutine and calculates the classical turning points, r_1 and r_2 required to integrate the Bohr-Sommerfeld relation. The turning points are found by checking at which values of r the expression $E'_L - V_T(r)$ changes sign, where E'_L is our guess at the energy of the state.

The program then integrates the left hand side of the Bohr-Sommerfeld relation by using a simple rectangular rule:

$$\int_{x_1}^{x_n} f(x)dx = \sum_{i=1}^{n-1} f(x_i)\Delta x$$

Sufficiently narrow spacing between consecutive points ($\Delta x = 0.001$ fm) yields accurate results for the integration.

The computed integral is compared to the right hand side of the Bohr-Sommerfeld relation. According to the difference between the two values, the *energy* subroutine then either ends and returns the value for $E_L(\text{Theor}) = E'_L$ (if the value of the LHS is within a certain error margin of the RHS), or it adjusts the value of E'_L accordingly and restarts the *energy* subroutine to recalculate the classical turning points and perform the integration again.

Once the energy levels $E_L(\text{Theor})$ of the entire band for the given value of R have been calculated, the value of the following expression is determined:

$$S = \sum_L [E_L(\text{Expt}) - E_L(\text{Theor})]^2$$

where $E_L(\text{Expt})$ is the value of the L^{th} experimental energy level and $E_L(\text{Theor})$ is the value of the L^{th} energy level as determined above.

The program then cycles through a grid of 20 values $R \rightarrow R + dR$, and finds the value of R which minimises the sum of squares S. From this a new starting value of R and a new step size dR are calculated and the main program runs again for 20 values of R. In this way the program refines its search for the best fit energy level spectrum until R is determined up to 6 significant figures.